Comptes Rendus

Physique

Jonathan Amodeo and Laurent Pizzagalli

Modeling the mechanical properties of nanoparticles: a review

Plasticity and Solid State Physics / *Plasticité et Physique des Solides*

Modeling the mechanical properties of nanoparticles: a review

Jonathan Amodeo [a, b] **and Laurent Pizzagalli**[*, c]

[a] Université de Lyon, INSA-Lyon, MATEIS, UMR 5510 CNRS, 69621 Villeurbanne, France

[b] Aix Marseille Univ., Université de Toulon, CNRS, IM2NP, Marseille, France

[c] Departement of Physics and Mechanics of Materials, Institut P′, CNRS UPR 3346, Université de Poitiers, SP2MI, Boulevard Marie et Pierre Curie, TSA 41123, 86073 Poitiers Cedex 9, France

E-mails: jonathan.amodeo@insa-lyon.fr (J. Amodeo), laurent.pizzagalli@univ-poitiers.fr (L. Pizzagalli)

Abstract. Nanoparticles are commonly used in various fields of applications such as electronics, catalysis or engineering where they can be subjected to a certain amount of stress leading to structural instabilities or irreversible damages. In contrast with bulk materials, nanoparticles can sustain extremely high stresses (in the GPa range) and ductility, even in the case of originally brittle materials. This review article focuses on the modeling of the mechanical properties of nanoparticles, with an emphasis on elementary deformation processes. Various simulation methods are described, from classical molecular dynamics calculations, the best suited method when applied to the modeling the mechanics of nanoparticles, to dislocation dynamics based hybrid methodologies. We detail the mechanical behaviour of nanoparticles for a large array of material classes (metals, semi-conductors, ceramics, etc.), as well as their deformation processes. Regular crystalline nanoparticles are addressed, as well as more complex systems such as nanoporous or core-shell particles. In addition to the exhaustive review on the recent works published on the topic, challenges and future trends are proposed, providing solid foundations for forthcoming investigations.

Keywords. Nanoparticles, Mechanical properties, Plastic deformation, Dislocations, Numerical simulations.

Available online 21st May 2021

1. Introduction

Nanoparticles (NPs) are pieces of solid matter whose three dimensions range typically from a few to several hundreds of nanometers. Research on their properties and potential applications is a well-established and active domain of materials science and of nanotechnology, as evidenced by the impressive numbers of related published papers or organized conferences every year. NPs are

---

* Corresponding author.

characterized by a large surface-to-volume ratio, as well as by potential quantum confinement effects for the smallest specimens. The prevailing role of surfaces leads to specific structural, electronic, optical, chemical and magnetic properties compared to bulk materials [1,2]. Furthermore surfaces can be functionalized, allowing to tune properties or to open the way to new features as e.g., light emitting devices [3], imagery and drug/gene delivery in biomedicine [4] or catalysis [5], to mention just a few. NPs are often characterized by improved mechanical properties when compared to the corresponding bulk materials. This makes them interesting prospects for improving the tribological properties of lubricants, as well as for strengthening nanocomposite materials [6]. Dedicated experimental investigations, usually conducted using nanoindentation techniques [7,8], allowed to reveal a list of key features. Firstly, it appears that NPs could be much stronger than bulk materials [9–19]. For instance, Gerberich and coworkers found that 20–50 nm silicon nanospheres are characterized by a hardness ranging from 20 to 50 GPa [9]. More recently an impressive 34 GPa compression strength value was determined for 210 nm Ni NPs [18]. A similar "smaller is stronger" tenet has been largely documented for larger systems such as micropillars, though usually with lower strength values [20,21]. It is now agreed that the size effect at the microscale is essentially related to the reduction of available volume for dislocation source operation [22–25]. In the smallest systems, at the nanoscale, a significantly different kind of plasticity based on a nucleation process takes place.

Another interesting observation is the increase of fracture toughness when the NP size is decreased [26]. Small enough NPs made of brittle materials like silicon or magnesium oxide can indeed be deformed plastically [15,27,28]. In the specific case of silicon, the hindering of fracture at small scale has potentially important implications for battery applications [29]. Note that such a phenomenon was already substantiated for microparticles made of inhomogeneous materials [30], but not in the case of quasi perfect crystal NPs. We will come back to it later.

Finally, distinctive plasticity mechanisms could operate in NPs compared to the bulk. Hence the competition between dislocation mediated plasticity and twinning in metallic NPs is expected to depend on the size, as for grains in nanostructured materials [31]. In semiconductor NPs at room temperature, Wagner and coworkers recently reported partial dislocation plasticity [32], which only occurs at high temperature in bulk [33]. Also unusual slip systems and phase transformations were also observed in nanopillars [17,34]. All these mechanisms are a likely consequence of the high stresses reached at small scales [35].

As with nanopillars, the size is a critical parameter for NP mechanical properties. It influences the shape and the crystalline structure of NPs, the presence of preexisting defects and flaws, and also stress concentration buildups under load. However, the NP shape should probably be considered as an equally important parameter for mechanical properties. In fact, it directly influences the nature of free and contact surfaces, since a NP can be cubic (therefore equivalent to a nanowire with a square section and an aspect ratio of 1) but also spherical or polygonal. Furthermore the NP crystalline structure as well as the internal stress buildups also depend on the shape, which could therefore impact the mechanical properties.

Available experimental results on the mechanics of NPs were essentially obtained by compression and indentation, which are the only simple loading mode applicable to NPs. It is notoriously difficult to spatially or temporally resolve the initiation and development of the plastic deformation in these experiments, because of the small sizes and the occurrence of strain bursts. Modeling at the atomic or dislocation level then appears as an ideal complement, which can provide detailed information about the activated processes and their dynamics. This asset has motivated a significant number of investigations during the last decade. The goal of the present article is to review these works, thus providing a synthesis for future research projects in the field. We focus here on the mechanical properties of NPs obtained from several modeling approaches, from density functional theory (DFT) simulations to the finite-element method (FEM), with a particular
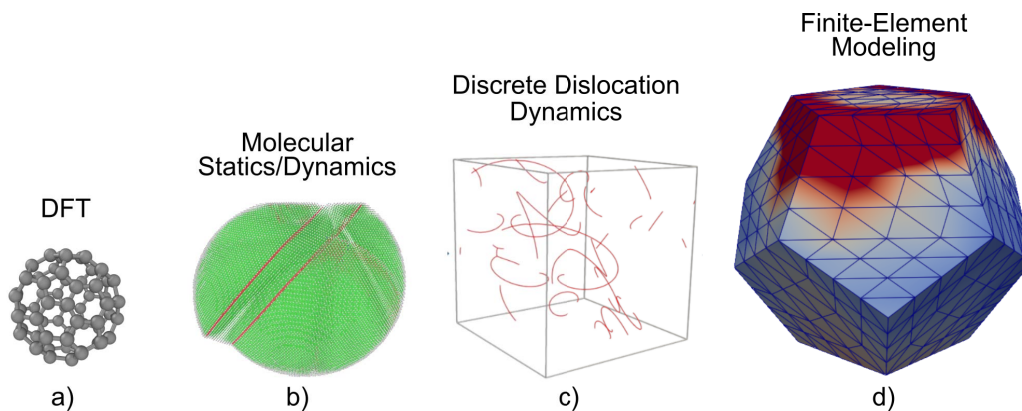
Figure 1. Simulation methods currently used to model nanoparticle mechanics with typical examples including (a) DFT simulations of the compression of a C_{60} molecule, (b) Nanocompression of a Ni NP using atomistic simulation (atoms in FCC environment are colored in green, HCP atoms in red), (c) DDD simulation of a MgO nanocube under compression and (d) Von Mises stress distribution during the compression of a dodecahedron metal nanoparticle using FEM.

focus on molecular dynamics (MD) simulations that is for now the most appropriate technique to investigate NP mechanics.

This paper is organized as follows. In the next section, an overview of the theoretical and practical concepts of the simulation methods applied to NP mechanics is made. Section 3 synthesizes the results on the elasticity and strength of NPs, and in particular on how they depend on the NP size, shape, and materials. In Section 4, we review the various plasticity mechanisms occurring in crystalline NPs as revealed by numerical simulations. The available results associated with NPs with a non-crystalline state or with a special structure (core-shell, hollow) are described in Section 5. Finally, in the last section, general conclusions about the current state of the art are drawn, followed by a list of challenges that should be (and will be, hopefully) overcome in the future.

2. How to model the mechanics of nanoparticles?

Although the interest in modeling NPs mechanics is quite recent, computational materials science techniques such as DFT, MD and molecular statics (MS), discrete dislocation dynamics (DDD) and FEM, have already been applied to the field (Figure 1). While DFT simulations are generally restricted to the investigation of small clusters of atoms (see [36–39] for examples), MD appears as the most popular modeling method due to its ability to describe atomic-scale elementary deformation processes (dislocation nucleation, twinning) in virtual samples with sizes comparable to the experiments.

2.1. *Atomistic simulations*

MS and MD are atomic-scale methods both based on classical mechanics. They make use of interatomic potentials that connect the energy of a subset of atoms (pair, triplet or more) to interatomic intrinsic properties (distance, angles, charges, etc.). In MS simulations, the local energy minimum of a system is computed from convergence algorithms such as the conjugate

gradient, the Hessian-free truncated Newton method or damped dynamics algorithms [40–42]. Various spatial configurations of atoms are consecutively tested during the energy minimisation in a time-independent manner. As a consequence, velocities and accelerations of atoms are not defined in MS simulations i.e., MS are static, 0K-like, simulations. While the outcome of MS appears as a single minimum energy configuration, the method can still be used in an iterative manner e.g., to mimic a NP compression test, applied strain or stress being increased between each energy minimisation. This approach, called "quasi-static simulation", has been rarely used to investigate NPs properties. In the same way, minimum energy path methods such as the nudged-elastic-band (NEB) [40] or the activation-relaxation technique (ART) [43] that focus on optimizing configuration trajectories (from an initial to a final state) are not often applied to NP mechanics modeling but usually to the cases of nanowires or pillars [44–46]. From our knowledge, NEB was only recently used to compute the site dependence of dislocation nucleation activation barrier, at the surface of ceramic nanoparticles [47].

MD simulations focus on integrating the displacement of atoms along time. The second Newton's law is integrated using a Verlet-like algorithm to derive $t + 1$ velocities and positions. Thus, dynamic runs (equilibration, compression or tensile tests) can easily be performed with MD assuming the correct setup of a few parameters, such as the integration timestep that is commonly about a few fs i.e., a fraction of the atomic vibration period. Assuming a CPU time per MD step that scales with the number of atoms, it is obvious that the MD physical time (generally about 1–100 ns) can not be compared to usual experimental timescales that are of a few seconds or minutes in the case of NPs compression tests. To offset the timescale issue and achieve a significant amount of strain during a virtual nanomechanical test, MD simulations are usually performed at extremely high strain rates i.e., in the 10^7–10^9/s range, way over experimental conditions of deformation. While it is known to have only a limited impact on the elastic deformation of NPs, it can significantly influence the elementary deformation processes and the nucleation stress. Despite this potential artifact, as it will be discussed in the next sections, MD was regularly employed to investigate various kinds of NPs including crystalline metals, ceramics and semi-conductors, providing valuable piece of information about NP deformation processes necessary to interpret *in situ* TEM and SEM experiments.

2.2. *Nanomechanics using MD*

As mentioned in the introduction, nanoindentation and nanocompression are the two main experimental tests developed to probe NP mechanical properties. Both make use of an indenter tip (made out of diamond, sapphire or tungsten carbide), that can either indent the flat top surface of a faceted NP directly (see e.g., the work of Kovalenko *et al.* [48]), or after etching leading to the so-called "flat punch" shape used for nanocompression [15, 32]. Both tests were modeled by MD using mainly two approaches for the design of indenter and substrate: (i) the "frozen atoms" approach and (ii) the "virtual force field" approach. While both approaches rely on the application of a force field on surface and subsurface NP atoms, they are slightly different in terms of applied mechanical constraints. On the one hand, in the "frozen atoms" approach, the user simply designs a flat punch, a spherical or a Berkovitch indenter, made out of an infinitely tough, *frozen*, group of atoms. This last feature is easily achieved in whatever MD code cancelling the forces acting on these atoms or not accounting for them during time integration. Thus, the rigid block of atoms yields a repulsive force field (at short distance) that will be used to compress the NP. In this case, the compression force can be retrieved from the atomic interactions between the NP and the *frozen* block atoms. On the other hand, the "virtual force field" approach makes use of an explicit analytical formulation of a directional force field. For example, in the popular LAMMPS code [49], one can set a virtual indenter using a force defined by $F(r) = -K(r - R)^2$,

Figure 2. Nanosphere with rough surfaces designed for atomistic simulations using spherical harmonics.

where K is a rigidity constant and $(r - R)$ the distance between the indenter position R and the atoms that depends on the indenter shape. In the case of a flat punch, the LAMMPS indenter is axis-aligned and infinite. It acts as a wall that exerts the same repulsive force on every atoms that are at same $(r - R)$ distance from the wall. The main difference between both approaches relies on the directional aspect of the force fields i.e., the "virtual force field" approach is generally axis-aligned while the use of a rigid block of atoms leads to multi-directional as well as additional attractive forces.

Nanoindentation experiments are characterized either by displacement- or load-controlled setups [50, 51]. For the sake of simplicity, the displacement-controlled model is preferred in MD nanocompression simulations even if a load-controlled feedback loop could easily be implemented. A displacement-controlled simulation is designed by imposing a displacement of a given amplitude per MD step to the indenter. As a consequence, stress-strain curves modeled by MD are characterized by stress loads and drops similar to those observed in displacement-control experiments at the nanoscale. At first order, displacement-controlled simulations can be compared to load-controlled experiments if accounting for stress-strain curve maxima only [10]. However, one can note that stress instabilities are not observed in load-controlled experiments that rely on smoother dislocation dynamics.

2.3. *Stress and strain definitions*

The force *vs.* displacement curve is the "fingerprint" of the NP mechanical response. It is the most straightforward outcome to get from a nanocompression experiment and is particularly used in MD or FEM simulations, especially in the case of spherical NPs for which the elastic properties can be fitted with the Hertz model [52, 53]. Force *vs.* displacement experimental data can be transposed into stress and strain assuming some knowledge about sample dimension variations (contact surface and height), affordable using e.g., the digital image correlation (DIC) technique. While engineering and true strains are easily retrieved from nanocompression simulation (either from the instantaneous position of the indenter or height of the NP), the stress definition is more challenging (see discussion in [54], when applied to MD nanocompression tests). Thanks to the cumulative work done on micropillars, we know that the compressive stress i.e., the force

recorded by a sensor divided by the contact surface, is the relevant observable for nanocompression tests as the near contact region is where most of plasticity events start from (assuming the lack of subsequent extrinsic stress concentrators). While the contact force is a direct outcome of both experiments and simulations, the contact surface is more complex to measure. In *in situ* experiments, the initial dimensions of a NP can be measured using a SEM/TEM camera to define the engineering compressive stresses. More recently, the DIC method was used to calculate *on-the-fly* NP dimensions when compressed inside the TEM (see e.g., [15]). Nevertheless, DIC measures rely on 2D-side projections that only allow for NP edge length measurements, and not for the top surface area that is only approximated in this case. However, several methods exist to determine top surface area in MD nanocompression tests. The most simple ones rely on the initial sample (or simulation cell) shape and dimensions to deduce the engineering stress. To go further and measure the true stress, one can monitor the box dimension changes assuming the use of shrink-wrapped boundary conditions. However, this method remains approximate as it does not rely on the real shape of the NP and neglects the possible surface shape changes induced by localized and heterogeneous plastic events (e.g., nanotwinning). A more precise method consists in computing rigorously the NP top surface area based on the atomic positions. This can be done using the Delaunay triangulation of the atomic positions as shown e.g., in [54, 55]. These last approaches can be combined to a probe sphere method to account for irregular contacts [55] as e.g., for nanoporous or rough surfaces. While this last method might be precise, one can argue about its connection to experiments, where such details in the contacts cannot yet be reached.

2.4. *NP design*

NPs are characterized by various shapes such as sphere, cube or faceted shapes (polyhedrons), that rely on both the material considered and the fabrication route. In the simulations, simple "cutting" algorithms are commonly used to model basic shapes, including faceted NPs retrieved from e.g., the Wulff theory. While this approach allows for various NP designs, it suffers from several drawbacks such as surface flatness and particularly sharp edges. Hybrid approaches using various theories (roughness, spherical harmonics) as well as a combination of meshing and atomistic simulation tools can also be used (see e.g., Figure 2). The influence of the sample design on the mechanical properties at the nanoscale being more and more discussed in the atomistic simulation community, several authors tried to build more realistic samples including the use of a blunting parameter [54, 56] or extruding some of the edge atoms [18], to round NPs edges and corners. Pre-heating up to a significant amount of the melting temperature is also performed to allow NPs surface reorganisation and integrate randomness in MD simulations [57, 58]. In the literature, few experimental methods such as X-ray tomography and atom probe allow to gain information about the sample geometry that can be used in the simulation [59–61]. However, while the resolution of the X-ray tomography is restricted to larger scale simulations such as FEM, atom probe is very difficult to apply to nano-objects (especially NPs) due to the needle-like processing of the sample. Up to now, Bragg coherent diffraction [62] and TEM (together with DIC) are the only methods able to characterize NPs surface and shape with a resolution close to the nm. From the authors' knowledge, these methods are not yet used for the design of NPs in simulations due to their complexity.

2.5. *DDD and FEM models*

One of the major drawbacks of atomistic simulations is the CPU cost per modeled volume quantity. Indeed, MD requires the computation of typically hundreds of thousands of atomic interactions per time step, which constrains the NP size to a few tens of nanometers (on regular super-
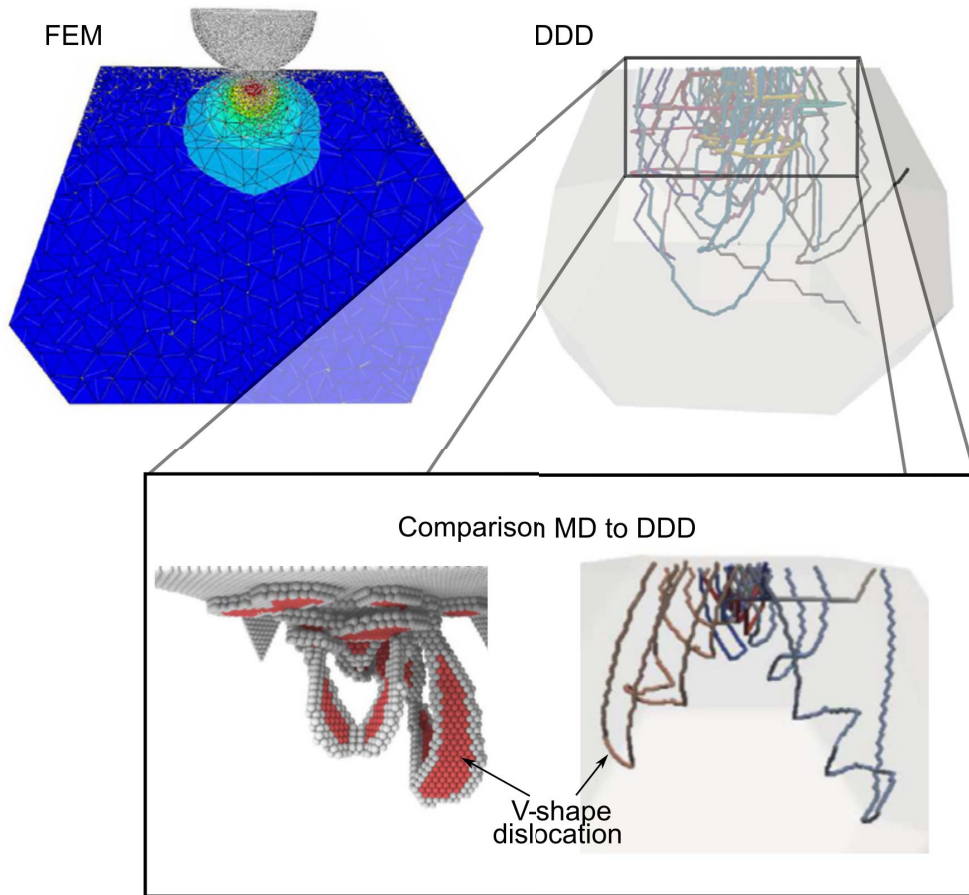
Figure 3. ⟨111⟩-nanoindentation simulation of an Au nanoparticle. Comparison between MD and an hybrid DDD/FEM approach. Adapted from Roy *et al.* [63] with permission.

calculators). To offset this problem, upscaling using the mesoscale DDD technique can be performed [64–67]. In DDD, the elementary brick is not the atom but a dislocation portion (segment or node). Due to the smaller number of objects to model (dislocations fragments or nodes may represent hundreds or thousands of atoms), DDD allows to model sample with sizes up to a few μm on a larger timescale than in MD (from the μs to the ms). DDD relies on the calculation of dislocation interactions under an applied stress based on the elastic theory, assuming an infinite continuum media. In Roy *et al.* [63], the authors used DDD to model the indentation of a metal NP for which the heterogeneous stress field is imported from a FEM simulation (see Figure 3). Using a dislocation nucleation procedure, they successfully compared parts of incipient elementary deformation processes (V-shaped dislocation and prismatic loops) to those of classical MD simulations. Nevertheless, the authors confirmed the inaccuracy of the sole DDD to mimic parts of the dislocation multiplication processes observed in MD, mainly due to the lack of glissile junctions in their model. Furthermore, classical DDD simulations suffer from the lack of surfaces and do not account for image forces that can influence the dislocation dynamics in NPs. One possibility to bypass the image force problem is to couple the DDD to another approach to correctly tackle the boundary problem. Several hybrid methods exist and the most commonly used are the superposition method [68, 69] and the Discrete-Continuous Model (DCM) [70–73]. The super-
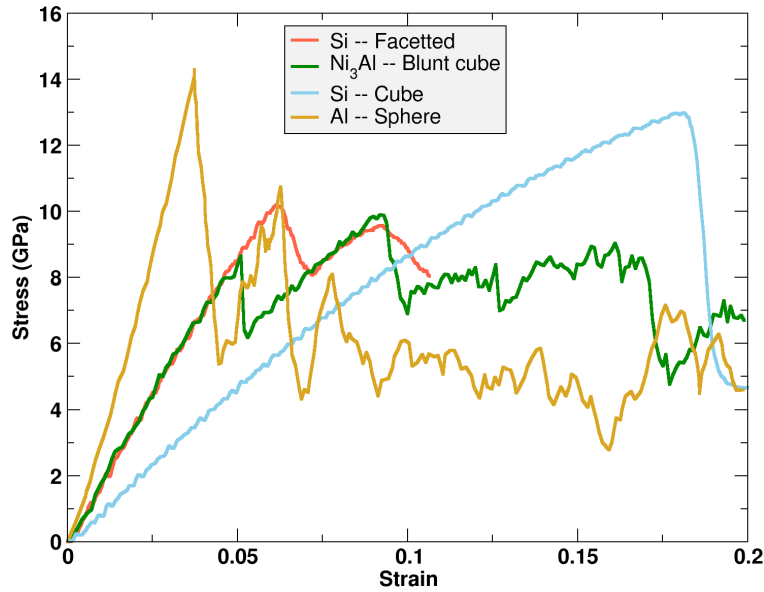
Figure 4. Compressive stress as a function of strain for MD nanocompression simulations of various NPs, retrieved from the literature (True stress: red curve [56], light blue curve [56], goldenrod curve [84]. Engineering stress: green curve [54]).

position method relies on the correction of the load applied to a finite-size sample (computed by FEM) accounting for the stress and displacement fields induced by a dislocation population (computed by DDD, in an infinite elastic medium) to solve a boundary condition problem (for example: relax free-surfaces). In contrast with classical DDD, the superposition method allows for heterogeneous loads and a more realistic description of the influence of surfaces/interfaces on the mechanics. On the other side, dislocations in the DCM are modelled as plate-like inclusions related to an eigenstrain field [74] in an elastic medium. Within the DCM, the DDD code only focuses on regularising the plastic strain (from slipped areas) and short-range dislocation interactions, the FEM calculating the associated stress field further used to drive the next DDD simulation step. In contrast with the superposition method, long-range dislocation interactions are computed by the FE code in the DCM. From our knowledge, while both methods were used to model nanoindentation tests [69,75], composite materials and alloys [76,77], crack initiation and propagation [78,79] as well as deformation of pillars, wires and thin films, at the micro- and nanoscales (see e.g., [80–83]), they have not been applied yet to investigate the mechanics of NPs. Obviously, mesoscale hybrid simulations such as the superposition method or the DCM would be of great help to better assess the mechanical properties and elementary deformation processes of NPs. Indeed, these methods would allow to reach sizes, strain rate and timescales closer to experimental tests, in contrast with atomistic methods.

3. Nanoparticles under compression: probing the strength of crystalline nanoparticles

As mentioned in the previous section, stress and strain can easily be retrieved from any nanocompression simulation while taking into account the contact force and area as well as geometry variations. Figure 4 shows a few examples of stress–strain curves for different kinds of NP. Common characteristics to all curves are high stress values and a first monotonic regime extending over a
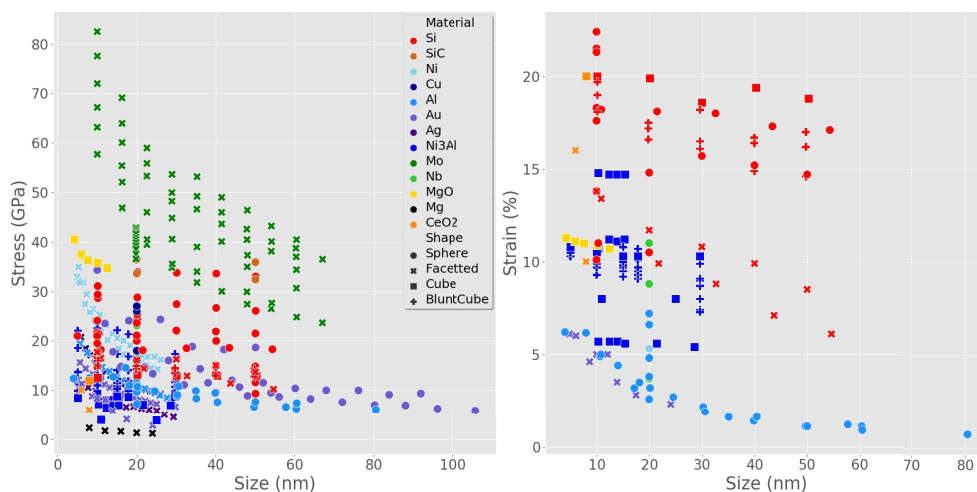
Figure 5. Maximum compressive stress (left) and associated strain (right) computed during uniaxial compression of NPs, as a function of the size, modeled by MD. Markers and their colors represent the NP shape and materials. Data compiled for Si [56, 90–94], SiC [90], Ni [55, 95], Cu [52, 95, 96], Al [84, 95], Au [10, 95, 97], Ag [95], Ni$_3$Al [54, 98, 99], Mo [100, 101], Nb [102], MgO [15], Mg [103], CeO$_2$ [58]. Note that reported stress values often correspond to true stresses, with a minority of them being engineering stresses.

large strain range, for instance up to 0.17 for the cubic Si NP. Stress variations are initially linear, albeit with significant deviations for large strains. This reflects the non-linear character of elasticity at large strains, in addition to the widening of contact surfaces during compression. Small serrations are usually observed in this regime, due to thermal fluctuations of the contact forces and surface areas, and eventually small rearrangements of atoms at contact surfaces and edges.

It is possible to determine elastic moduli from the linear part of a stress–strain curve, although they are often not reported in the literature. It is not clear whether such a modulus would be dependent on the NP size except for very small systems where surfaces dominate [85, 86]. The elastic modulus of a NP is equivalent to the Young modulus only when the cross section is constant along the compression axis and therefore equal to the contact surface. This is true for a perfect nanocube for instance, but not for Wulff-like faceted or spherical shapes NPs. In the latter cases, the strain/stress fields inside the NP are not homogeneous [87], and the slope of the strain–stress curves becomes necessarily size- and shape-dependent. It makes the determination of a well-defined elastic modulus a questionable goal. Note that additional issues arise in the case of spherical NPs. In fact the atomistic character of the contact dominates for low NP sizes [85,88,89], and the contact surface area at small deformation may also depend on the way the spherical model is built for a specific orientation. As an alternative to the elastic modulus, one could determine the stiffness during compression i.e., the slope of the load-displacement curve, which allows to avoid the aforementioned issues. However, this quantity is explicitly dependent on size, and can not be used to investigate a possible size effect on elastic properties.

The end of the elastic regime is marked by significant stress drops on the stress–strain curves (Figure 4). These drops are associated with mechanisms like dislocation nucleation or phase change, which will be described with more details in the next section. It is tempting to define the yield stress as the maximum stress reached before the first stress drop. However it could be misleading in the case of NPs, since it has been reported that seemingly apparent plastic deformations could be reversible [52, 104, 105]. The strength of the NP is usually defined as

the maximum stress reached during the compression. It is also sometimes called hardness by analogy with nanoindentation experiments [9]. Figure 5 represents the strength of various NP systems plotted as a function of NP size and organized according to the NP material and shape as modeled with MD. The studied materials are primarily FCC metals, silicon, and molybdenum, with additional data for another BCC metal (Nb), an intermetallic alloy (Ni_3Al), a covalent alloy (SiC), an oxide (MgO), and an HCP metal (Mg). Although most of the data correspond to NP sizes below 50 nm, large spherical NP with diameters of at most 106 nm have been investigated [97]. The most striking observation from this figure pertains to the large range of computed values, from about 1 GPa to 82 GPa, with a significant proportion above 20 GPa. The highest strengths are obtained for faceted Mo and cubic MgO NPs, followed by Si and SiC nanospheres. Strengths for FCC NPs tend to be generally lower. Exceptions include the smallest Ni NPs, for which values greater than 30 GPa were reported [95]. In all cases, it is clear that the NPs appear much stronger than their bulk counterparts. Figure 5 also shows the elastic strain limit corresponding to the maximum stress, when available in the literature. Critical strains ranging from about 1% to 24% were predicted, with the highest values for silicon NPs. The spectacular strength of NPs is a direct consequence of such an extended elastic regime.

NP nanocompression MD simulations are typically carried out with strain rates that are several orders of magnitude larger than in experiments. This is known to influence the initiation of plasticity, especially at high temperatures [44, 106]. Other potential differences concern the models used in atomistic simulations, which are usually akin to perfect geometrical shapes unlike real NPs. Furthermore, defects can be introduced in the NP due to fabrication and impurities layers present at its surface. Finally, a cause for discrepancies is related to the use of classical interatomic potentials, which are usually parameterized against bulk properties and may describe NP surfaces and edges with a low accuracy. It is important to keep these limitations in mind before comparing simulations and experiments. Considering available data, we find four possible cases. First, there could be an apparently good agreement between calculated strengths and experimental values, despite at least one order of magnitude size difference between the models and the real NP. This happens for Mo [101], Ni [18], Au [10], Ni_3Al [12, 107], Mg [103], and Ag [108]. This size discrepancy is not easily explained. The absence of a size effect might be a clue in the case of cubic NPs [12, 15, 107]. A possible size threshold below which the strength remains constant has also been suggested [16], although this argument conflicts with the size effect obtained in both experiments and calculations [10, 101]. Finally, a fortuitous agreement is always possible. As will be discussed below, the shape and the surface state could have a major influence on the mechanical response, and the design of simulated NPs might be too simple when compared to real systems as already discussed. A second case includes measurements performed on NPs with dimensions comparable to simulated ones, but yielding strength values smaller than in simulations [13, 14]. Large uncertainties can not be excluded since sizes are 13–22 nm in these studies. Third, a commendable agreement, both for size and stress, is observed for silicon NPs. In fact, Gerberich and co-workers reported maximum stresses ranging from about 4 to 30 GPa for spherical NPs with diameters between 60 and 130 nm [26, 109], and from 9 to 14 GPa for cubic NPs with sizes between 22 and 69 nm [32]. These values are similar to those determined from simulations [56]. The last case includes materials where both reported NP sizes and compressive stresses are different, and for which it is therefore difficult to draw conclusions. For instance, in 80–120 nm MgO nanocubes, Issa *et al.* [15] measured yield strengths in the 1–5 GPa range from *in situ* TEM nanocompression, while MD simulations predicted larger strengths (35–40 GPa) for smaller nanoparticles in the 10 nm range.

It is now acknowledged that the strength of pillars and nanowires increases when the size (diameter in that case) is reduced [21], and that in most cases this size effect is due to the shrinkage of space available for dislocation source operation [22–25]. Considering the data in
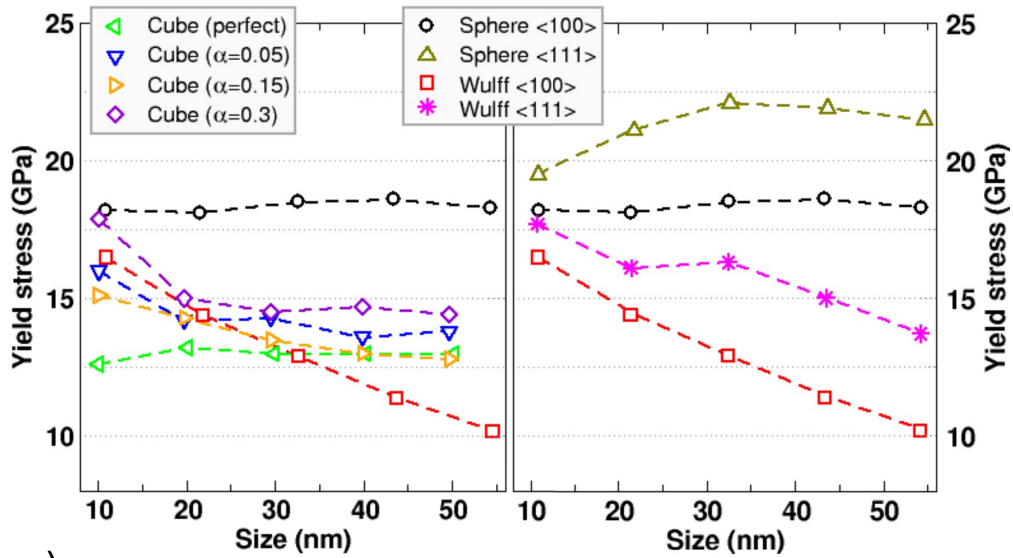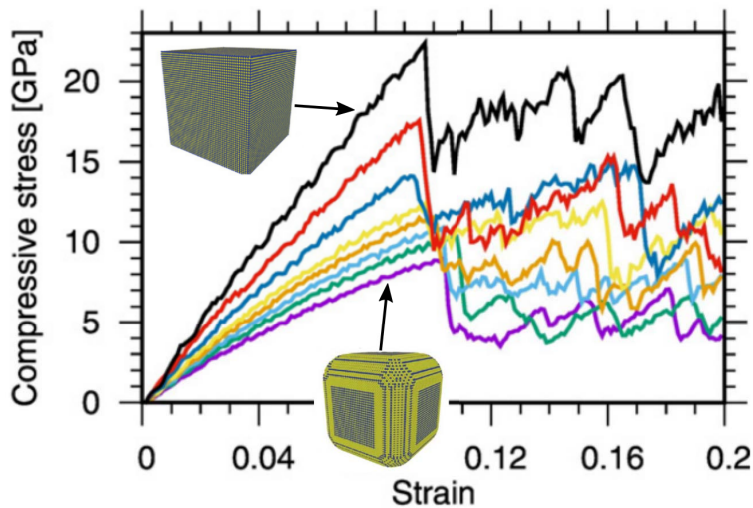
Figure 6. (a) Maximum stress as a function of size for silicon NPs, for different shapes and orientations (adapted from [56] with permission). α is the rounding coefficient applied to the particle edges and corners ($\alpha = 0$ for a perfect cube, and $\alpha = 1$ for a sphere). (b) Stress–strain curves associated with the compression of Ni$_3$Al cubic NPs, with α increasing from the top curve to the bottom one (adapted from [54] with permission).

Figure 5 as a whole, a universal size effect on the maximum stress appears unlikely (even using a logarithmic scale). However, focusing on data subsets for Mo and FCC metals, one can notice that small NPs tend to be stronger than the large ones. This size effect has been reported by Mordehai and co-workers in 2011. They found that the computed strength of gold NPs with Wulff-like shape follows a power law with an exponent of −0.74, very close to a measured exponent of −0.77 [10]. More recently, Feruz and Mordehai proposed that a similar law could be generalized to other FCC metals for the same NP shape, albeit with a different exponent value of −0.5 [95]. These NPs yield through the nucleation of dislocations from the vertices of the faceted NPs, and the size effect

is explained by the size-dependent buildup of stress gradients at these locations [110]. A similar explanation was put forward in the case of faceted "Wulff-like" silicon NPs [56], which also exhibit a strength-size dependence (Figure 6).

The size effect appears to be closely correlated to the faceted shape of FCC and Mo nanoparticles. In fact, the strength of cubic Si [56] and Ni_3Al [98] NPs does not depend on size, although plasticity also initiates by nucleation of dislocations from the vertices. It has been suggested that the cubic shape does not allow for the concentration of stress at cube corners [56, 110], thus suppressing the size dependence observed for faceted NPs. However, it is noteworthy that Issa and co-workers found a weak size dependence for the strength of cubic MgO NPs (see [15] and Figure 5), which is maybe specific to this ionic material. Nanospheres constitute another well studied class of NPs, for which the relation between strength and size also depends on the studied materials, conversely to faceted and cubic NPs. In fact, Yang *et al.* observed a "smaller is stronger" trend for gold NPs [97], while several studies reported a size independent strength for silicon NPs [56, 90, 94] (Figure 6). A potential cause for this discrepancy is that incipient plasticity initiates from the surface for gold, whereas it occurs inside the NP for silicon (see the next section for an in-depth discussion of plasticity mechanisms). In the former case, it has been demonstrated that the structure of the surface in contact with the indenter, like the width of terraces delimited by atomic steps for instance, directly influences the initiation of plasticity [97, 105].

The influence of shape on mechanical properties of NPs has been thoroughly investigated by Kilymis and co-workers [56]. Figure 6a represents the maximum stress versus the size of Si NPs, for different shapes. The stress is seemingly not dependent on size for spherical and perfect cubic NPs. Conversely a well-defined size effect is obtained for faceted NPs. Amodeo and Lizoul also found that the maximum stress reached during the compression of Ni_3Al NPs critically depends on the rounding level of the cube [54]. Hence the strength of the perfect cube is more than twice that of a blunt cube (Figure 6b). These two results suggest that the mechanical response of compressed NPs depends more on their shape than on their size. Furthermore, they also highlight the need to use models with geometries as close as possible to the real NPs, if meaningful comparisons between calculations and experiments are expected.

4. Plastic deformation processes in crystalline nanoparticles

4.1. *Nano-ductility*

Thus, decreasing size makes particles stronger. While this paradigm has attracted a substantial attention since the early-2000s and the work of Uchic *et al.* [20], it has been known for more than four decades that materials get stronger and even more ductile when smaller leading to a size-induced brittle-to-ductile transition (BDT) [30, 111, 112]. Kendall [30] demonstrated how the cracking force of a particle quickly rises as the particle size decreases below a critical value using a simple approach derived from the Griffith energy criterion. The conditions required for breakage rely on the elastic energy availability in the system i.e., under a certain size and a too low amount of elastic energy to relax, the material has no other choice but to plastically deform. While the Kendall model leads to mm-size transition in polymers, it is close or below the μm for originally brittle materials such as chlorides or oxides. So at first order, the critical size for the BDT only depends on the critical stress intensity factor K_{IC} and hardness H of the material [113]. Gerberich and co-workers also showed how the fracture toughness of silicon increases when the size is lowered [26, 28]. Thus, failure is generally postponed to larger strains in NPs (when compared to the bulk material) leaving room to a more ductile behavior. In the following, we will thus mostly focus on the elementary plastic deformation processes occurring in NPs rather than on breakage.

The plastic deformation of NPs is firstly driven by dislocation nucleation processes. Indeed, while bulk material engineering relies on managing dislocation multiplication and their mean-free path playing with defects contents, NPs, that benefit from soft fabrication routes (such as epitaxy deposition or dewetting), are generally dislocation-free meaning that *something* has to nucleate to initiate the plastic deformation. The question of this *something* depends on the material and possibly on the NP size: mostly dislocations (either partial or perfect) but also nanotwins or new phases (including amorphized domains). In fact, nucleation operates first in pristine NPs whatever the *something* is. In the following, we describe the most common plastic deformation processes happening in MD simulations of NPs compression tests, as reported in the literature. In particular, we focus on the nucleation process rather than on the following dislocation or twin dynamics, for which MD simulations are less relevant due to the high strain-rate.

4.2. *FCC metals*

Most of the literature content about modeling mechanics of NPs concerns monoatomic metals, with a particular focus on FCC metals where $1/6\langle 112\rangle\{111\}$ partial dislocations nucleate first, generally from the surface of the sample [10, 52, 55, 95, 102, 105, 114]. Due to the high symmetry of the NP design in MD simulations, several partial dislocations can nucleate simultaneously from a unique nucleation region (i.e., in different slip systems) or from different edges or corners of the NP. When the compression axis is along $\langle 100\rangle$, the first event leads to the formation of a pyramidal dislocation structure (Figure 7a) located in the indenter sub-region due to a simultaneous activation of three slip systems (see e.g., [52]). The first nucleation event can be followed by various elementary deformation processes such as the nucleation of subsequent partial dislocations and nanotwinning (Figures 7b–c). Feruz and Mordehai [95] investigated several FCC metal faceted NPs under $\langle 111\rangle$ compression using MD and highlighted the various mechanisms operating after the nucleation of the first Shockley dislocation: (i) nucleation of a correlated trailing partial as in Au (also observed in [10]) or (ii) nucleation of a subsequent leading partial in an adjacent slip plane leading to the formation of an extrinsic stacking fault (nanotwin embryo) as observed in Cu, Ni (confirmed in [55]) and Ag. These various processes are shown Figures 7d–i. Despite the wide set of FCC metal NPs investigated, the authors did not observe any explicit correlation between material properties (in particular, the stacking fault energy) and the related dislocation process. As compared to the rest of the literature, Cu shows various activated processes as nanotwins in Wulff-shaped NPs with compression axis along $\langle 111\rangle$ [95] and $\langle 100\rangle$-oriented nanospheres [52] or the nucleation of correlated partial dislocations in $\langle 111\rangle$-oriented nanospheres [52]. These results confirm that, unlike nanocrystalline materials [115], a stacking fault energy-based criterion is not enough for dislocation nucleation in FCC NPs, and that a detailed analysis of the influence of the contact region, the shape and size of the NP, on the stress concentration, is required.

4.3. *BCC and HCP metals*

BCC NPs were recently studied and show a more anisotropic plastic response when compared to FCC. Faceted Fe NPs compressed using MD along $\langle 110\rangle$ deform due to usual $1/2\langle 111\rangle\{110\}$ perfect dislocations [116]. For this orientation, the $1/2\langle 111\rangle\{112\}$ slip systems exhibit the maximum resolved shear stress (larger than for $1/2\langle 111\rangle\{110\}$) and is chosen to interpret compression experiments of Mo NPs using FEM simulations [101], while MD compressions in Mo NPs show a dislocation activity in both $1/2\langle 111\rangle\{112\}$ and $1/2\langle 111\rangle\{110\}$ slip systems [100, 117]. Bian and colleagues have investigated BCC NPs anisotropy by means of a set of MD compression simulations on BCC Nb nanospheres with compression axis along $\langle 110\rangle$, $\langle 111\rangle$ and $\langle 100\rangle$ [102]. Results
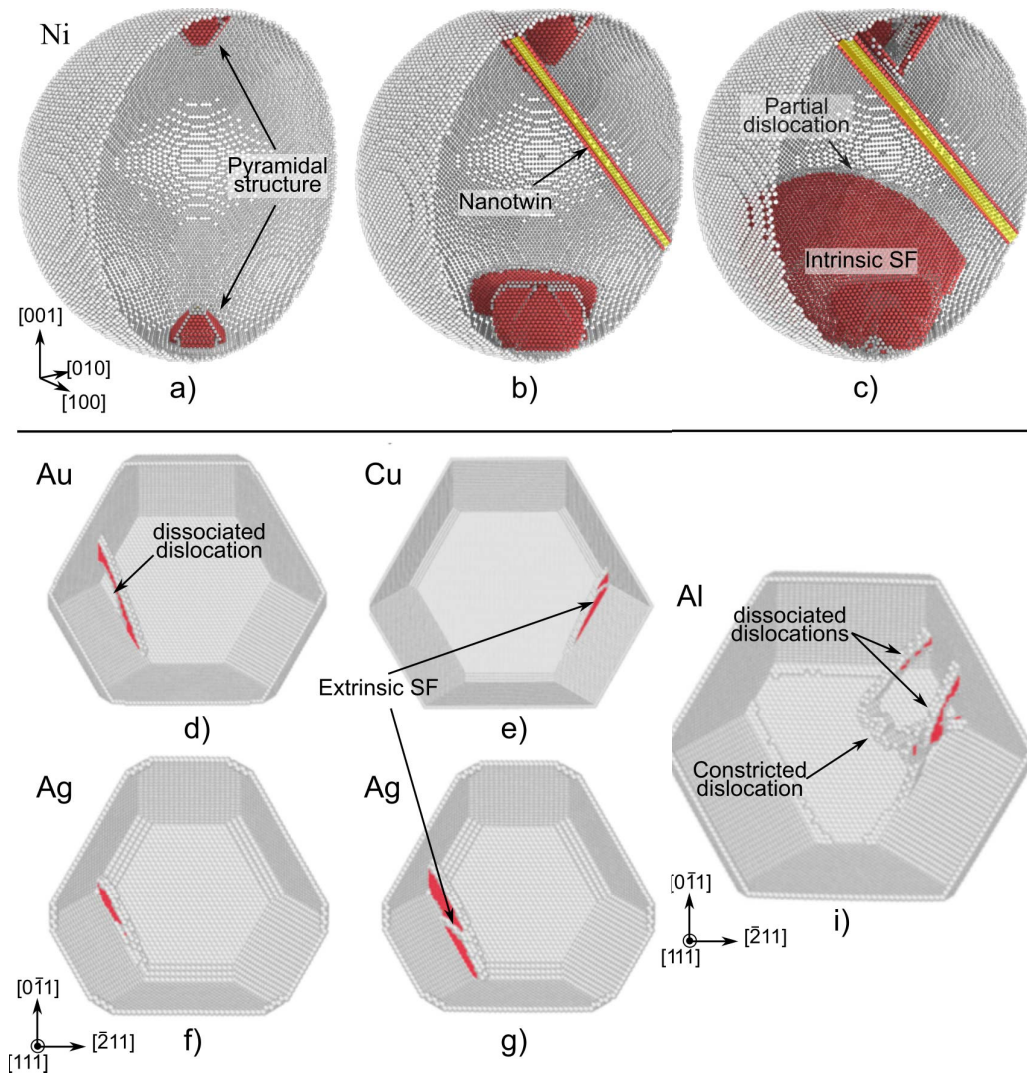
Figure 7. Dislocation nucleation and nanotwinning in FCC nanoparticles compressed using MD. (a) Nucleation of a pyramidal structure of dislocations from indenter/substrate sub-regions in a 20 nm Ni nanosphere compressed along ⟨100⟩, (b) nucleation and propagation of a nanotwin (yellow domain), (c) further nucleation events. (d)–(i) Various dislocation nucleation processes in Au, Cu, Ag and Al nanoparticles compressed along ⟨111⟩. Perfect crystal atoms are removed for a sake of clarity. Surface and defective atoms are colored in light-grey. Atoms in HCP environment are in red. Adapted from [55] and [95] with permission.

emphasize the versatility of BCC NPs elementary deformation processes including 1/2⟨111⟩{110} dislocation slip for ⟨110⟩ compression axis, ⟨111⟩{112} twinning for ⟨111⟩ compression axis and a combined activation of ⟨111⟩{110} twinning (twinning direction) along with ⟨111⟩{110} dislocation slip (anti-twinning direction) for ⟨100⟩ compression axis (Figure 8). As recalled by the authors, these mechanisms can be significantly different (even if using the same modeling method) than from other nano-objects or bulk, as is the case for BCC tungsten nanopillars that show twin-
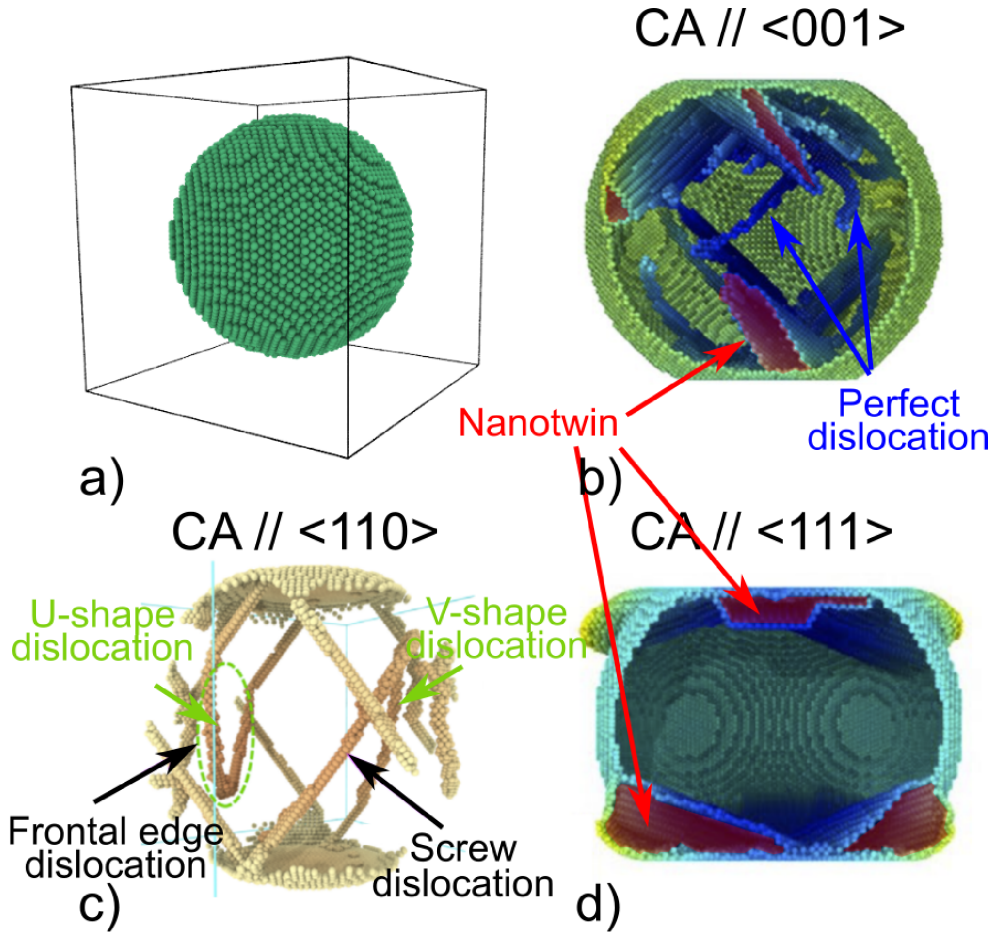
Figure 8. BCC niobium nanoparticle under compression using MD, (a) Perfect 10 nm diameter niobium nanoparticle, (b)–(d) Elementary deformation processes occurring during compression with compression axis (CA) along ⟨001⟩, ⟨110⟩ and ⟨111⟩ respectively. Perfect crystal atoms are removed for a sake of clarity. Adapted with authors permission from the work published in [102].

ning for ⟨110⟩ compression axis [118]. As it has long been discussed, the plastic deformation of bulk BCC materials can not be easily pictured (when compared to FCC), due to the combined complexity of the BCC screw dislocation core and glide processes, that are now known to be sensitive to the stress environment (non-Schmid effects) [119–123]. In this context, one can easily understand the versatility of the elementary deformation processes observed in BCC NPs that are characterized by a shape-dependent internal stress field distribution in addition to the aforementioned BCC peculiarities.

From our knowledge, less is known about HCP metal NPs except for the study of Yu *et al.* [103] that investigates a size-dependent transition from ⟨a⟩-type dislocation (large particles) to multiple types of dislocation sources (smaller particles, in the 100 nm range) in Mg faceted NPs. Nevertheless, while the deformation processes were addressed thanks to *in situ* TEM nanocompression, MD simulations only account for size-effect on strength without much investigations on dislocation slip.

4.4. *Ni$_3$Al*

Concerning alloys, a careful consideration was given to ⟨100⟩-oriented Ni$_3$Al nanocubes for their role as strengthening main constituent of γ/γ' superalloys [54, 98, 99]. Ni$_3$Al exhibits the L1$_2$ crystal structure i.e., a binary FCC-like structure with Ni atoms at mid-surface positions [124]. As a consequence, Ni$_3$Al plastic deformation relies on ⟨110⟩{111} superdislocation with a Burgers vector twice larger than in usual FCC metals [125, 126]. Several splitting schemes for the superdislocation were proposed in the literature, including a sequence where the ⟨111⟩ superdislocation dissociates into two 1/2⟨111⟩ called superpartials (separated by an anti-phase boundary) which split again into two 1/6⟨112⟩ Shockley partials each, with a complex stacking fault extending between each Shockley partial dislocation that makes each superpartial. While {111} octahedral slip is known to be replaced by {100} cubic slip at higher temperature in Ni$_3$Al [125, 126], microtwinning is also observed in the γ' phase under intermediate temperature and high-stress conditions of deformation [127, 128]. The first MD studies focusing on dislocation nucleation in Ni$_3$Al sharp nanocubes [98, 99] showed the nucleation of 1/6⟨112⟩{111} Shockley partial dislocations and complex stacking faults from the corners and side edges of the nanocubes, later leading to pseudo-twinning as the main deformation process (regular Ni$_3$Al twinning but without the Ni/Al reshuffling, see [127] for details). Furthermore, Amodeo and Lizoul verified the aforementioned full splitting sequence (including the occurrence of anti-phase boundaries) altogether with the same pseudo-twinning process in nanocubes with rounded edges and corners, designed closely to the experimental samples [54]. Again, this last study emphasizes the role of the contact surface and its consequence on deformation processes (e.g., heterogeneous versus homogeneous nucleation, see discussion later) due to the induced stress concentration.

4.5. *Semiconductors*

The literature on the plasticity mechanisms operating in semiconductor NPs is mainly focused on silicon, which is also the covalent material with the most complete information on bulk plasticity [33]. In a nutshell, there are two dislocation families in bulk silicon, with partial 30° and 90° dislocations in so-called "glide" {111} planes at high temperatures, and undissociated perfect dislocations with various characters in "shuffle" {111} planes at low temperatures [129, 130]. One can expect to observe the second kind of these dislocations in NPs, since investigations have been essentially made at ambient conditions. However, it is also noteworthy that bulk silicon is prone to phase transformations (β-tin, amorphization) at lower pressures than those occurring during the compression of NP (see Section 3).

Most of published works concern spherical silicon NPs compressed along the ⟨100⟩ orientation. It does not help to reach a conclusive picture for this case though. Some studies report the homogeneous nucleation of perfect shuffle dislocation loops in regions located beneath the indenter [56, 93, 131, 132] (Figure 9a). Others rather indicate that a β-tin phase transformation occurs [92, 94, 131] (Figure 9b). The reason for this disagreement is probably the use of different interatomic potentials, and is one of the most important issue to overcome for a better understanding of silicon NP plasticity using atomistic simulations. The same problem arises for the ⟨111⟩ orientation. Hong *et al.* find the formation of a metastable tetragonal phase (seemingly different from β-tin according to the authors) using a Tersoff potential, whereas the homogeneous nucleation of perfect dislocations occurs when using a modified Stillinger–Weber potential [56]. Finally, it also seems that amorphization becomes the most likely plasticity mechanism below a certain NP size [131, 133]. This might be due to the hindering of dislocation nucleation in the limited available volume, or the tendency of crystalline surfaces towards disorder when dimensions decrease.
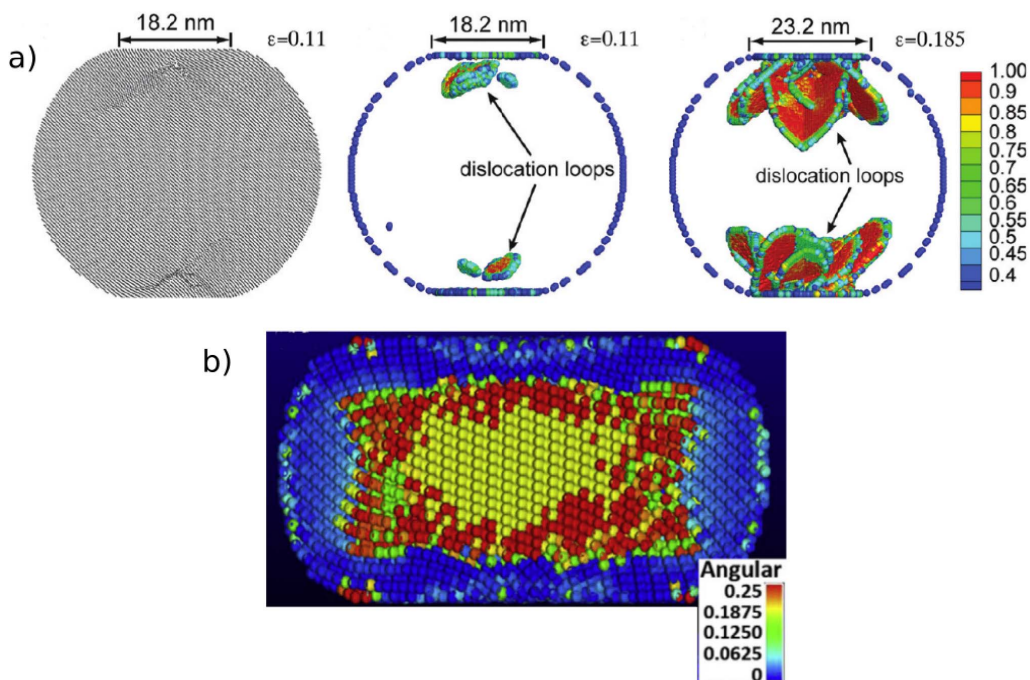
Figure 9. Si NPs compressed using MD simulations. (a) 40 nm spherical NP deformed at 11% (left and middle image) and 18.5% (right image), showing the homogenenous nucleation and expansion of dislocation loops (slip vector representation) in the vicinity of the contact surfaces (adapted from [131] with permission). (b) Formation of a β-tin phase (yellow atoms) in the center of a 10 nm spherical NP after unloading following a $\langle 100 \rangle$ compression (adapted from [92] with permission).

The influence of the NP shape on the plasticity mechanisms was investigated in details by Kilymis an co-workers [56], again revealing a complex situation. In faceted NPs and for a $\langle 100 \rangle$ oriented compression, plastic deformation occurs by the heterogeneous nucleation at edges of shuffle perfect dislocations, simultaneously gliding in two different {111} planes. These V-shape dislocations could be explained by the bi-axial stress condition developing at the contact surface during compression [134]. However, shifting to a $\langle 111 \rangle$ oriented compression, it was found that the faceted NP yields by the nucleation and propagation of a superpartial dislocations. These dislocations might be similar to those experimentally observed during the compression of nano-objects [32, 34]. Furthermore, the formation of superpartial dislocations in silicon was recently correlated to the presence of large compression stresses [35]. Kilymis *et al.* also considered cubic NPs of various sizes, and found that most of them tend to plastically deform through the heterogeneous nucleation of dislocations at corners [56]. However, these perfect dislocations glide in {110} planes instead of {111}. This behavior is also predicted to occur in nanowires with a square section and is also apparently a consequence of the high stresses reached during compression [135].

Then it appears that the plastic deformation mechanisms predicted by atomistic simulations in Si NPs largely depend on the shape, the size, and the orientation. But it is also related to the interatomic potential used for these simulations. This is a severe issue which could undermine the validity of these predictions, and calls for additional investigations in assessing the reliability of available potentials in high stress conditions and in the development of more accurate potentials for Si.

4.6. *Ceramics*

Finally, a few crystalline ceramic NPs were also studied recently in the light of applications in materials engineering (sintering of nanocrystalline ceramics) and catalysis. In particular, ⟨100⟩-oriented MgO nanocubes were deformed using *in situ* TEM nanocompression and MD simulations [15]. MgO is a model ceramic with the B1 rock-salt structure used to develop experimental protocols and models that later apply to more complex systems [136]. MgO bulk single crystals are characterized by dislocation slip in 1/2⟨110⟩{110} and 1/2⟨110⟩{100}, respectively activated at low and large shear stresses [137–140]. In MgO NP compression simulations, perfect 1/2⟨110⟩{110} dislocations were observed to nucleate from the corners and edges of the nanocubes, providing solid foundations for the interpretation of the 45° slip traces observed *in situ* in TEM experiments. These results are in good agreement with γ-surface calculations in low-Miller index planes that allows for a first order picture of dislocation nucleation in the rock-salt structure [15]. In addition, Amodeo and colleagues [47] performed NEB simulations to investigate the site dependence of dislocation nucleation activation energy at the surface of MgO nanocubes. Their results confirm the corners and edges propensity to 1/2⟨110⟩{110} nucleation including a full-mapping of activation energy and nucleation frequency at various temperatures.

CeO$_2$ is another ceramics widely investigated for its ability to store and release oxygen (via a reduction of CeO$_2$ ceria into Ce$_2$O$_3$), crucial for catalysis applications. Most of the atomistic simulations related to the mechanics of ceria nano-objects (NPs, but also wires) were made by Sayle and collaborators (see e.g., [57, 58, 141–144]). CeO$_2$ exhibits the (cubic) fluorite structure i.e., a combination of two cerium FCC and oxygen simple cubic sublattices. In contrast with MgO NPs that are mostly cubic-shaped, CeO$_2$ NPs can exhibit various geometries, including truncated octahedrons, polyhedrons and cubes (or cuboids), due to the instability of the fluorite {100} surfaces. Thus, to simplify the numerical sample design, the Sayle's group developed an amorphization/crystallization method either leading to polycrystalline polyhedral NPs (see e.g., [57]) or single crystalline cuboïdal NPs when making use of an original cubic-shape seed [58], in agreement with TEM observations. Sizes of modelled NPs are below the 10 nm range. MD compression simulations show that the plastic deformation of single crystalline CeO$_2$ NPs is first controlled by an amorphization process before the first dislocation nucleation event takes place, whereas polycristalline NPs show grain boundary-mediated plasticity (including $\Sigma 3$ and $\Sigma 11$) and Ostwald ripening.

Finally, α-alumina Al$_2$O$_3$ nanospheres were also investigated using MD simulations [145]. α-alumina is a renowned ceramics that exhibits a complex HCP structure (30 atoms per unit cell), particularly used for biomedical applications [146]. In this study, the authors performed MD compression simulations of 10 nm α-alumina single- and bi-crystalline NPs along the ⟨0001⟩ direction to interpret TEM observations. While single crystals deform by rhombohedral {1$\bar{1}$02} slip, a typical slip system of bulk alumina, bi-crystals with a grain boundary parallel to compression axis yield by void nucleation and fracture (Figure 10). These results confirm experimental results in which large NPs containing pre-existing defects as dislocations and grain boundaries are more prone to crack than lower-sized pristine NPs.

4.7. *Nucleation and multiplication*

Overall, this special kind of deformation is referred to as "nucleation-controlled plasticity" in the literature, especially when related to dislocation or twinning. The nucleation process generally operates from defective regions as surfaces that behave as sources for the heterogeneous dislocation nucleation process or for phase transformation initiation. Nevertheless, rare cases of homogeneous nucleation were also recently discussed in NPs [18, 54, 56]. Homogeneous nucleation in NPs emerges from stress concentration that relies in part on the global shape of the
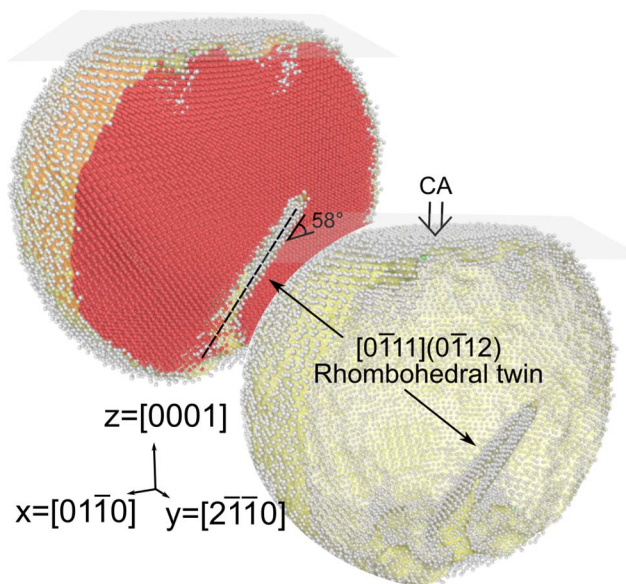
Figure 10. Rhombohedral twinning in a α-Al$_2$O$_3$ nanosphere under $\langle 0001 \rangle$ MD compression. Top left: O atoms are shown in red (HCP environment). Al atoms are not shown. Surfaces and defective regions as twin boundaries are shown by atoms colored in light-grey and yellow area (interfaces). Bottom right: only surface and defective region atoms are shown for a sake of clarity.

NP. While nanocubes exhibit homogeneous stress distribution, it is not the case of faceted NPs or even nanospheres that show more spread stress distributions (see e.g., Figure 12 in [56] for a shape-dependent picture of the von Mises stress in NPs using MD or Figure 5 in [101] for a FEM picture of stress heterogeneity in rounded NPs). It also relies on the local contact between the modeled indenter and the surface of the NP. As discussed e.g., in [54], when the indenter contacts the top of the NP during nanocompression, the top first layers of atoms are elastically shifted downward, compressing those underneath. Depending on each layer area, this process can lead to local stress concentration and underlayer bending responsible for a progressive increase of shear stress, layer after layer, inside the NP. Nevertheless, the heterogeneous *vs.* homogeneous dislocation nucleation process is still under debate in NPs. For example, while the compression of $\langle 100 \rangle$-oriented Si and Nb nanospheres leads to homogeneous dislocation nucleation [56, 102], it is not the case for similarly oriented Cu and Al NPs that exhibit nucleation from the surface [52, 105]. Thus, a more in-depth investigation of the parameters responsible for the heterogeneous-to-homogeneous nucleation transition is required to optimize models as those proposed in [54, 97, 105].

Finally, from an experimental point of view, raising the size of NPs up to 1 or several hundreds of nm reduces the possibility to get them pristine. Indeed, large NPs often contain pre-existing dislocations (see e.g., [147]) that should help to promote plastic deformation, in a similar manner as to what happens in nano- and micropillars. Jennings *et al.* [148] emphasized a dislocation nucleation-to-multiplication transition in Cu nanopillars increasing the diameter of the sample in the 100 nm range (depending on the strain rate) using SEM compression experiments. Thus, as for other nano-objects, NPs should be characterized by a size-dependent transition from dislocation nucleation to multiplication which has, to our knowledge, not been discussed in the literature up to now (at least from a modeling point of view).
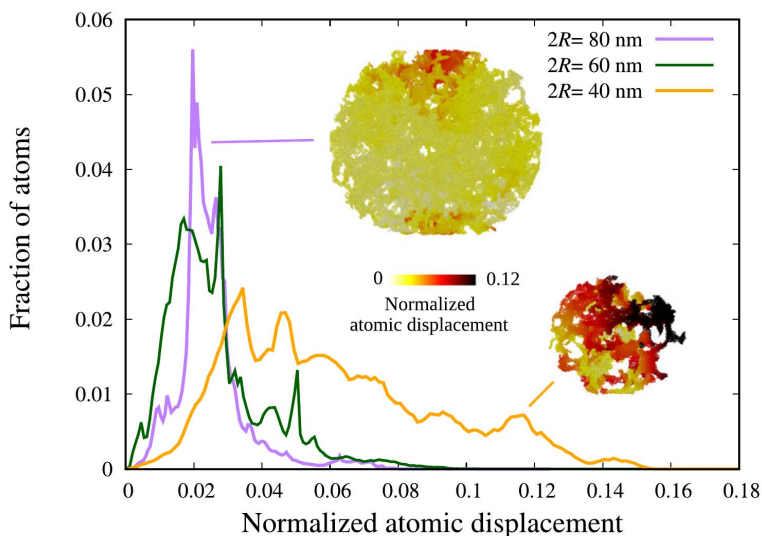
Figure 11. Distribution of atomic displacements, normalized by the size, in highly porous silica nanospheres, for a compression strain of 0.15. This figure shows that the plastic deformation becomes more homogeneous when the NP size decreases. Reproduced from [158] with permission.

5. Mechanics of nanoparticles with non-crystalline or complex structures

In the previous section we focused on single-crystalline NPs, which concern most of published works. Here, we discuss the available results on the mechanical properties of NPs made of amorphous materials, obtained from numerical simulations. Furthermore, experimental advances now allow to investigate more complex systems, such as core-shell, hollow, or nanostructured NPs [4, 149–157]. This section also includes the available information from numerical simulations for these NPs.

5.1. *Non-crystalline NPs*

A few atomistic simulations dedicated to the investigation of the mechanical properties of non-crystalline NPs recently appeared in literature. Compared to works reported in previous sections, only the spherical NPs were considered. These studies revealed several interesting and sometimes apparently contradictory features. For instance, Kilymis and co-workers investigated the mechanical properties of amorphous silicon NPs with two different diameters, 16 nm and 34 nm, averaged over 5 configurations for each size [159]. They found a maximum stress reduction of about 5–6% from large to small NPs, for two different temperatures i.e., smaller is softer, unlike for crystalline materials. The authors cautioned against a significant dispersion among stress–strains curves of all computed systems, which may deceptively amplify the stress difference. Issa *et al.* also reported a slight decrease of the stress associated with the strain hardening stage of the compression of silica NPs, when their diameter varies from 30 nm to 5 nm [160]. No prospective mechanisms causing this size effect have been suggested in both studies. The calculated stiffness of highly porous silica NPs was also shown to depend on size, with the softest response for the smallest systems [158]. The authors conclude that the increasing number of dangling ligaments at the NP surface leads to softer NPs for decreasing sizes. However, coarse-grained molecular dynamics investigations of the mechanical compression of polyethylene NPs show a different

picture, the stiffness increasing when the NP diameter decreases from 40 nm to 5 nm [161]. In this case, it is the increase of density close to the surface that is assumed to be the main factor. Finally, the size was shown to have little or no influence on the mechanical properties of carbon-based NPs, which might be due to the limited range of sizes investigated [162, 163]. The existence of a general size effect for the mechanical properties of non-crystalline NPs is therefore not clearly demonstrated on the basis of available simulations. The current information tends to suggest that this potential size effect could critically depend on multiple factors, like for instance the density and connectivity for polymer NPs. To a certain extent the size effect for non-crystalline NPs, if it exists, is likely material dependent.

Unlike crystals, the density of most disordered materials can be substantially altered by compression, and analysis were performed to determine the amount of densification. For silica NPs it is found that the density continuously increases up to 78% at a 0.9 strain [160]. A similar phenomenon occurred for highly porous silica NPs [158], and for diesel soot NPs, with a 50% densification at 0.6 strain for the latter [19, 164]. Successive compressions of these two systems allow to reach even higher densities as well as an increase of hardness [19, 158, 164]. In the case of soot NPs, it was proposed that this hardening is caused by a growing proportion of sp^3 hybridized carbon atoms [19, 164] during compression. The influence of cross-linking between the hydrocarbonated molecules constituting the soot was also recently put forward [163]. Conversely, for an already dense material like amorphous silicon, only a 2% density increase at a compression strain of 0.3 is observed [159]. In the latter case, the matter pushed by the flat-punch indenter tends to flow and escape from the sides.

The available literature includes limited in-depth information on mechanisms operating during the plastic deformation of non-crystalline NPs. Gonçalves *et al.* examined the structural evolution of highly porous silica NPs, and in particular the respective role of ligaments and interconnected regions in the mechanical response [158]. They also show that the deformation becomes more homogeneous as the NP size decreases (Figure 11). A seemingly opposite behavior is observed for a-Si NPs [159]. The compression yields an increase of 5-fold coordinated atoms, which are the main carriers for plastic deformation in amorphous silicon [165]. However, those appear to be homogeneously distributed in the NP, with no influence of the NP size [159]. Furthermore, plastic deformation proceeds without the formation of localized shear bands, unlike in bulk amorphous silicon [166].

5.2. *Core-shell and hollow nanoparticles*

Core-shell NPs offer additional challenges to investigate due to the large number of possible configurations obtained by combining two different materials. The width of the shell is also a new tunable parameter to account for. Among all possible combinations, there are two special cases of core-shell NPs. First, the shell can be very thin compared to the NP diameter i.e., it is akin to a coating. These shells can be added to protect the NP core in harsh environment or to bring new functionalities [4]. The shell could also be made of a native oxide layer covering the NPs, formed before the NP compression. A second special case includes hollow NPs, which could be considered as a core-shell NPs with a missing core.

The investigation of mechanical properties of core-shell NPs is a very recent research field, and the number of dedicated atomistic simulations is currently limited. Available works already reveal several interesting facts. First, it was shown that the shell thickness can significantly influence the elastic response. The stiffness of the compressed NPs depends on the relative proportion of materials constituting the core and the shell. Increasing the width of a shell made of a harder material than in the core makes the NP stiffer [90, 167–169] (Figure 13a). Conversely, the compression of a NP made of a crystalline Ni core covered by a softer amorphous Ni shell
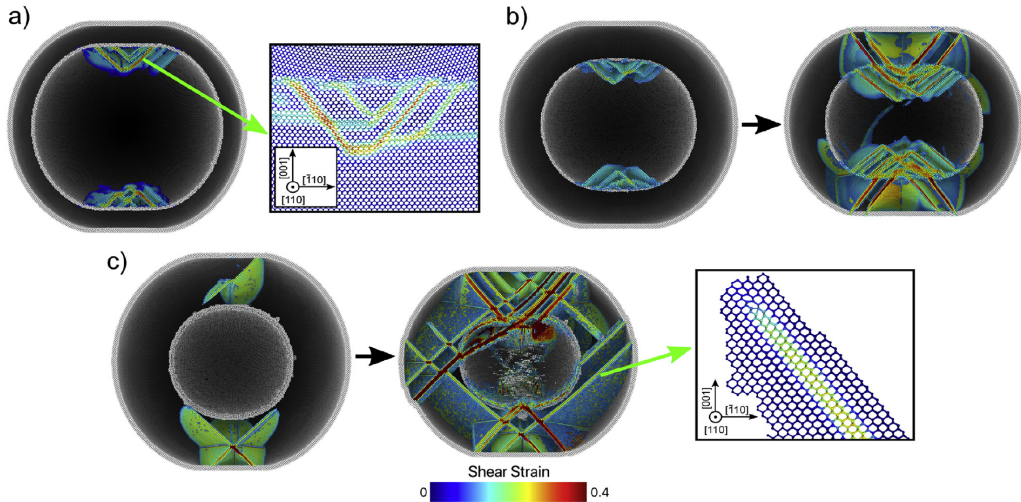
Figure 12. Cross-section views of compressed SiC/Si NP with a diameter of 50 nm and three different shell thickness (5 nm (a), 8.8 nm (b), and 12.5 nm (c)), at different compression strains. For clarity, perfect crystal atoms inside the NP are not shown. Other atoms are colored according to the computed von Mises shear strain. The two frames show slices of enlarged regions, revealing the structure of dislocation cores in shell and core regions. Reproduced from [90] with permission.

shows a softening compared to a pure crystalline Ni NP [55]. However, the elastic modulus does not vary with changing the shell thickness in that last case. The NP strength can also depend on the shell thickness [55, 90], as well as on the size of grains for a polycrystalline system [170].

A similar shell thickness effect was reported by Yang *et al.* for the specific case of hollow Si NPs [167]. The authors also proposed that there could be an optimal thickness value for which the strength could be higher than the full NP made of the same material, although no explanation for this behavior is given. Furthermore the hollow structure raises the apparent elasticity limit [167]. Such an increase of critical strains and stresses was also recently described for hollow NPs made of layered BN nanosheets [156]. Finally it is noteworthy that these results are in qualitative agreement with experiments performed on comparable hollow NP systems [154, 157, 171].

In addition to modifying mechanical quantities, it has been shown that the core-shell geometry has a significant influence on plasticity mechanisms. For instance, in the case of a single crystal NP, plastic deformation usually proceeds by nucleation of dislocations in the vicinity of the surface, close to the indenters (see previous section). For crystalline core-shell NPs, a dislocation mediated deformation is also observed, but nucleation can occur from either the surface or the core-shell interface, or both [90]. For a 50 nm Si/SiC NPs, Kilymis *et al.* showed that the shell thickness is the key selection parameter [90]. Dislocation nucleation occurs at the interface for a thin shell, while it occurs at the outer surface for a thick shell (Figure 12). The authors propose that surface nucleation could be hindered in NPs with thin shells due to the lack of enough available volume [90]. The compression of hollow Si NPs leads to an equivalent scenario, dislocations nucleating from either the outer or the inner surfaces depending on the shell thickness [167]. Finally, the presence of an amorphous layer coating a Ni NP has been shown to influence plastic deformation, with dislocations nucleating from the a-Ni/c-Ni interface at high sheared sites instead of below the indenter like in uncoated Ni NPs [55].
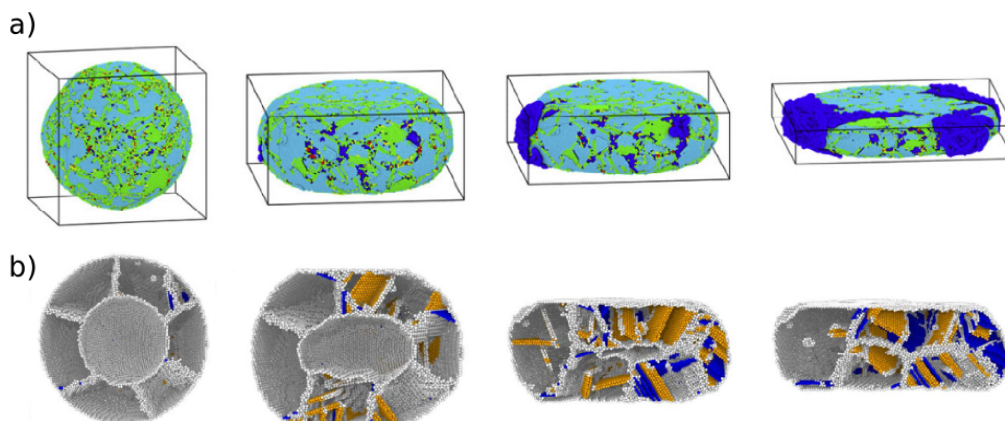
Figure 13. (a) 20 nm polyethylene nanospheres (CH$_x$ beads in blue) coated with a 0.5 nm thick Ni layer (green atoms), at different compression (Adapted from [168] with permission). (b) Cross-section views of polycrystalline hollow 20 nm Pd nanoparticles with a grain size of 10 nm and a shell thickness of 5 nm, at different compression strains. White atoms correspond to the grain boundary region, and the inner/outer surfaces. Orange and blue atoms depict atoms belonging to SF and twin boundaries, respectively (Adapted from [170] with permission).

Other plasticity mechanisms have been reported in core-shell NPs, including amorphization and phase transition. Hence, Yang *et al.* described the occurrence of small disordered regions during the buckling compression of hollow Si NPs with very thin shells [167]. Also, at high compression levels, the stacked hexagonal boron nitride layers forming a hollow NP transform to a zinc-blende phase [156]. Finally, in a recent investigation, Valencia *et al.* analyzed the plasticity mechanisms of hollow NPs made of polycrystalline palladium [170]. They found that grain migrations and rotations significantly contribute to the plastic deformation at all strains (Figure 13b).

6. Conclusions, challenges and future trends

6.1. *Conclusions*

The last decade has witnessed a significant amount of studies of the mechanical properties of NPs using numerical simulations. Diverse materials were considered, among which a majority of works dedicated to FCC metals and silicon. A synthesis of the results described in the preceding sections allows for drawing a few broad conclusions. First, a qualitative agreement between experiments and these simulations seems to be achieved. In fact, most studies come to the same conclusion that NPs are characterized by very high strength values, close or apparently higher than the theoretical strength of the bulk material [172]. The reasons are now well established and similar to the ones brought forward for nanowires: due the low available volume, NPs are close to be in a pristine state, with no or few pre-existing defects. Also, small volumes hinder plasticity mechanisms operating in the bulk. The effect, maybe even stronger in NPs than in nanowires or nanopillars, is mostly correctly captured by simulations, especially at the atomic scale. Extending the comparison between experiments and simulations to the strength values themselves, a good agreement is only obtained for a limited number of cases. This is somewhat not surprising given the differences between the real NPs and the models used in the simulations, or the use of interatomic potentials with limited accuracy at high stress for some classes of materials.

Undoubtedly, simulations are also interesting tools to supplement experiments. For instance a perfect control over the characteristics of the NPs is intrinsic to modeling. Furthermore, it allows for examining the influence of additional parameters such as the shape or the influence of the surface state in a statistical manner, especially with an increased repeatability when compared to experiments. Hence, available works demonstrated that the NP shape is as critical as the size when dealing with mechanical properties, and that it has a definite effect on the apparent strength size exponent and on activated plasticity mechanisms.

Another feature is the full access to the data produced during simulations. For example, positions and velocities of all atoms are known at each time step during the compression in a NP within a molecular dynamics simulation. It allows for an unequivocal identification of the plasticity mechanisms, which is more difficult to do in experiments. In this respect, several new mechanisms apparently specific to NPs, probably related to the high levels of involved stresses, have been discovered. This is especially true for silicon NPs. In FCC metals, the competition between dislocations mediated plasticity and twinning also seems largely dependent on the NP characteristics.

6.2. *Challenges and future trends*

Simulations of NP mechanical properties are unfortunately impeded by several issues, and finding ways to improve or circumvent each of those constitute challenges that should be overcome in the future. The first ones are related to size and time limitations of atomistic simulations. Thanks to the continuous growth of computational power and the development of efficiently parallelized simulation codes, at the time of writing of this paper it is possible to compute the dynamical compression of NPs with diameters of several tens of nanometers, containing millions of atoms, using empirical interatomic potentials. These sizes overlap with the smallest NP samples reported in experiments, allowing for a direct comparison. However, it would be interesting to model systems with sizes of a few hundreds of nanometers, which are common in these studies. Hopefully, such sizes will be accessible in the near future in atomistic simulations. Aside from the computation power increase, multiscale modeling techniques could also be interesting options. In that way, coarse-grained dynamics have already been used to model relatively small polymer particles [161]. Coupling atomistic calculations with DDD [173] could also have a great potential. Moreover, the development of DDD-based hybrid approaches (as coupled to FEM) could provide a valuable upgrade about the modeling of NPs mechanics, especially about the dislocation dynamics after yielding and the possible formation of dislocation microstructures inside the nanocrystal.

The physical timescale is a well-known limitation of most of the simulations. The gap between the standard strain rate and the one commonly used in these simulations is so large that it is doubtful it could be filled by solely relying on computational power growth. Several techniques have been developed aiming at extending the timescale accessible to atomistic simulations (see for instance [174, 175] and the chapter III in [176]). However, it remains to be seen whether these methods can be successfully used to investigate the mechanical properties of NPs. Being able to slow the compression rate closer to experimental levels would be extremely useful to ensure that the plasticity mechanisms observed in simulations are not critically dependent on the high strain rates.

Obviously, larger NP size and/or longer simulations would imply a substantial increase of the data produced during the calculations, which is already huge. For NPs with sizes of a few tens of nanometers and strain rates of 10^{-8} s^{-1}, it is hardly possible (and meaningless) to store all the information associated with a single compression MD run. Therefore, it is necessary to make clever guesses about the frequency at which the data should be recorded. Another option would

be to make as many analyses as possible during the course of the simulation [177]. Dealing with such a large amount of data certainly constitutes an issue for future investigations.

A last challenge is the availability of accurate potentials to describe interatomic interactions. They must be reliable enough to describe correctly highly distorted or specific atomic configurations as occurring in dislocation cores or at the NP surfaces/vertices, in high stress conditions. For FCC metals, it is now acknowledged that EAM-type potentials fulfill these criteria. Significant progresses have been made to describe BCC metals with these potentials too. However, for covalent materials and HCP metals, there is still room for improvement with respect to the available potentials. Potential prospects include machine learning potentials [178], which have been the subject of intense research recently. Although usually highly accurate, these potentials come with a substantial additional computational cost, that is currently prohibitive to deal with million atom systems. There is also a growing need to describe multicomponent systems, such as alloyed NPs, core-shell or coated NPs, for which there are often no available potentials. REAXXFF [179] or COMB [180] potentials have been developed specifically for this purpose, but again, the computational cost is much higher than with usual potentials. However, they might be useful to check the results obtained with simpler potentials for specific cases. Finally, for very small NPs, one might consider to use electronic structure methods like density functional tight binding [181], or even density functional theory [39].

As written before, one strength of simulations is the full control over the characteristics of the NP model. Although most of the reported works involve perfect shaped NPs with bare surface and pristine interior, it would be beneficial to try to make these models more realistic i.e., closer to experimental samples. For instance, Amodeo and Lizoul studied how the mechanical properties changed when cubic nanocrystals become more rounded and closer to real NP [54]. The latter can also exhibit surfaces with roughness, passivating impurities, oxidation, or disordered layers, which could noticeably influence mechanical properties. Furthermore, it is possible to introduce pre-existing defects into the bulk of the NP prior to compression. For instance, Kiani and co-workers showed that the behavior of compressed core-shell nanocubes was critically dependent on the presence of threading dislocations at the core-shell interface [182]. All these various aspects could be implemented in future simulations, and would help to develop a statistical theory taking into account the influence of surfaces and defects on the mechanical properties.

Finally, looking back at Figure 5, it appears that our knowledge is scarce for certain categories of materials. This includes for instance HCP metals, systems with a complex architecture like NP made of folded 2D layers, or NPs made of disordered materials. NPs made of brittle materials other than silicon or MgO are also insufficiently characterized, while they become more and more important in materials science engineering. Gaining further knowledge would maybe help to better understand the BDT transition occurring in these materials below a given size. Hopefully, these shortcomings will be remediated in the years to come.

Acknowledgements

References

[1] G. Schmidt, *Nanoparticles: From Theory to Application*, 2nd ed., Wiley, Weinheim, 2010.
[2] J. C. Nièpce, L. Pizzagalli, "Structure and phase transitions in nanocrystals", in *Nanomaterials and Nanochemistry*, Springer, Berlin, Heidelberg, 2007, p. 35-54.
[3] Z. Kang, Y. Liu, S.-T. Lee, "Small-sized silicon nanoparticles: new nanolights and nanocatalysts", *Nanoscale* **3** (2011), no. 3, p. 777-791.

[4] R. G. Chaudhuri, S. Paria, "Core/shell nanoparticles: classes, properties, synthesis mechanisms, characterization, and applications", *Chem. Rev.* **112** (2011), no. 4, p. 2373-2433.

[5] S. Fernández, L. Gao, J. P. Hofmann, J. Carnis, S. Labat, G. A. Chahine, A. J. F. van Hoof, M. W. G. M. T. Verhoeven, T. U. Schülli, E. J. M. Hensen, O. Thomas, M.-I. Richard, "In situ structural evolution of single particle model catalysts under ambient pressure reaction conditions", *Nanoscale* **43** (2019), no. 1, p. 331-338.

[6] D. Guo, G. Xie, J. Luo, "Mechanical properties of nanoparticles: basics and applications", *J. Phys. D: Appl. Phys.* **47** (2014), no. 11, article no. 013001.

[7] C. E. Carlton, P. J. Ferreira, "In situ TEM nanoindentation of nanoparticles", *Micron* **43** (2012), no. 11, p. 1134-1139.

[8] J. Deneen, W. M. Mook, A. Minor, W. W. Gerberich, C. B. Carter, "In situ deformation of silicon nanospheres", *J. Mater. Sci.* **41** (2006), no. 14, p. 4477-4483.

[9] W. W. Gerberich, W. M. Mook, C. R. Perrey, C. B. Carter, M. I. Baskes, R. Mukherjee, A. Gidwani, J. Heberlein, P. H. McMurry, S. L. Girshick, "Superhard silicon nanospheres", *J. Mech. Phys. Solids* **51** (2003), no. 6, p. 979-992.

[10] D. Mordehai, S.-W. Lee, B. Backes, D. J. Srolovitz, W. D. Nix, E. Rabkin, "Size effect in compression of single-crystal gold microparticles", *Acta Mater.* **59** (2011), no. 13, p. 5202-5215.

[11] D. D. Stauffer, A. Beaber, A. Wagner, O. Ugurlu, J. Nowak, K. A. Mkhoyan, S. Girshick, W. Gerberich, "Strain-hardening in submicron silicon pillars and spheres", *Acta Mater.* **60** (2012), no. 6-7, p. 2471-2478.

[12] R. Maaß, L. Meza, B. Gan, S. Tin, J. R. Greer, "Ultrahigh strength of dislocation-free Ni$_3$Al nanocubes", *Small* **8** (2012), no. 12, p. 1869-1875.

[13] M. Ramos, L. Ortiz-Jordan, A. Hurtado-Macias, S. Flores, J. Elizalde-Galindo, C. Rocha, B. Torres, M. Zarei-Chaleshtori, R. Chianelli, "Hardness and elastic modulus on six-fold symmetry gold nanoparticles", *Materials* **6** (2013), no. 1, p. 198-205.

[14] D. R. Saha, A. Mandal, S. Mitra, M. R. Mada, P. Boughton, S. Bandyopadhyay, D. Chakravorty, "Nanoindentation studies on silver nanoparticles", *AIP Conf. Proc.* **1536** (2013), no. 1, p. 257-258.

[15] I. Issa, J. Amodeo, J. Réthoré, L. Joly-Pottuz, C. Esnouf, J. Morthomas, M. Perez, J. Chevalier, K. Masenelli-Varlot, "In situ investigation of MgO nanocube deformation at room temperature", *Acta Mater.* **86** (2015), no. C, p. 295-304.

[16] W.-Z. Han, L. Huang, S. Ogata, H. Kimizuka, Z.-C. Yang, C. Weinberger, Q.-J. Li, B.-Y. Liu, X.-X. Zhang, J. Li, E. Ma, Z.-W. Shan, "From "smaller is stronger" to "size-independent strength plateau": towards measuring the ideal strength of iron", *Adv. Mater.* **27** (2015), no. 22, p. 3385-3390.

[17] E. Hintsala, A. Wagner, W. Gerberich, K. Mkhoyan, "The role of back stress in sub-50 nm Si nanocubes", *Scr. Mater.* **114** (2016), p. 51-55.

[18] A. Sharma, J. Hickman, N. Gazit, E. Rabkin, Y. Mishin, "Nickel nanoparticles set a new record of strength", *Nat. Commun.* **9** (2018), no. 1, p. 1-9.

[19] I. Z. Jenei, F. Dassenoy, T. Epicier, A. Khajeh, A. Martini, D. Uy, H. Ghaednia, A. Gangopadhyay, "Mechanical response of gasoline soot nanoparticles under compression: an in situ TEM study", *Tribol. Int.* **131** (2019), p. 446-453.

[20] M. D. Uchic, D. M. Dimiduk, J. N. Florando, W. D. Nix, "Sample dimensions influence strength and crystal plasticity", *Science* **305** (2004), no. 5686, p. 986-989.

[21] J. Greer, J. De Hosson, "Plasticity in small-sized metallic systems: intrinsic versus extrinsic size effect", *Prog. Mater. Sci.* **56** (2011), no. 6, p. 654-724.

[22] D. Kiener, A. M. Minor, "Source truncation and exhaustion: insights from quantitative in situ TEM tensile testing", *Nano Lett.* **11** (2011), no. 9, p. 3816-3820.

[23] F. Mompiou, M. Legros, A. Sedlmayr, D. S. Gianola, D. Caillard, O. Kraft, "Source-based strengthening of sub-micrometer Al fibers", *Acta Mater.* **60** (2012), no. 3, p. 977-983.

[24] D. J. Dunstan, A. J. Bushby, "The scaling exponent in the size effect of small scale plastic deformation", *Int. J. Plast.* **40** (2013), no. C, p. 152-162.

[25] P. S. Phani, K. E. Johanns, E. P. George, G. M. Pharr, "A simple stochastic model for yielding in specimens with limited number of dislocations", *Acta Mater.* **61** (2013), no. 7, p. 2489-2499.

[26] A. Beaber, J. Nowak, O. Ugurlu, W. Mook, S. Girshick, R. Ballarini, W. Gerberich, "Smaller is tougher", *Phil. Mag.* **91** (2011), no. 7-9, p. 1179-1189.

[27] W. Mook, J. Nowak, C. Perrey, C. Carter, R. Mukherjee, S. Girshick, P. McMurry, W. Gerberich, "Compressive stress effects on nanoparticle modulus and fracture", *Phys. Rev. B* **75** (2007), no. 21, article no. 214112.

[28] W. W. Gerberich, D. D. Stauffer, A. R. Beaber, N. I. Tymiak, "A brittleness transition in silicon due to scale", *J. Mater. Res.* **27** (2012), p. 552-561.

[29] M. T. McDowell, S. W. Lee, J. T. Harris, B. A. Korgel, C. Wang, W. D. Nix, Y. Cui, "In situ TEM of two-phase lithiation of amorphous silicon nanospheres", *Nano Lett.* **13** (2013), no. 2, p. 758-764.

[30] K. Kendall, "The impossibility of comminuting small particles by compression", *Nature* **272** (1978), no. 5655, p. 710-711.

[31] M. Chen, E. Ma, K. J. Hemker, H. Sheng, Y. Wang, X. Cheng, "Deformation twinning in nanocrystalline aluminum", *Science* **300** (2003), no. 5623, p. 1275-1277.

[32] A. J. Wagner, E. D. Hintsala, P. Kumar, W. W. Gerberich, K. A. Mkhoyan, "Mechanisms of plasticity in near-theoretical strength sub-100nm Si nanocubes", *Acta Mater.* **100** (2015), no. C, p. 256-265.

[33] J. Rabier, L. Pizzagalli, J.-L. Demenet, "Dislocations in silicon at high stress", in *Dislocation in Solids* (L. Kubin, J. P. Hirth, eds.), vol. 16, Elsevier, 2010, p. 47-108.

[34] A. Merabet, M. Texier, C. Tromas, S. Brochard, L. Pizzagalli, L. Thilly, J. Rabier, A. Talneau, Y. M. Le Vaillant, O. Thomas, J. Godet, "Low-temperature intrinsic plasticity in silicon at small scales", *Acta Mater.* **161** (2018), p. 54-60.

[35] L. Pizzagalli, J. Godet, S. Brochard, H. J. Gotsis, T. Albaret, "Stacking fault formation created by plastic deformation at low temperature and small scales in silicon", *Phys. Rev. Mater.* **4** (2020), no. 9, article no. 093603.

[36] R. Cherian, C. Gerard, P. Mahadevan, N. T. Cuong, R. Maezono, "Size dependence of the bulk modulus of semiconductor nanocrystals from first-principles calculations", *Phys. Rev. B* **82** (2010), article no. 235321.

[37] M. Cococcioni, F. Mauri, G. Ceder, N. Marzari, "Electronic-enthalpy functional for finite systems under pressure", *Phys. Rev. Lett.* **94** (2005), no. 14, article no. 093603.

[38] P. Maioli, T. Stoll, H. E. Sauceda, I. Valencia, A. Demessence, F. Bertorelle, A. Crut, F. Vallée, I. L. Garzón, G. Cerullo, N. D. Fatti, "Mechanical vibrations of atomically defined metal clusters: from nano- to molecular-size oscillators", *Nano Lett.* **18** (2018), no. 11, p. 6842-6849.

[39] L. Pizzagalli, "Finite-temperature mechanical properties of nanostructures with first-principles accuracy", *Phys. Rev. B* **102** (2020), no. 9, article no. 094102.

[40] H. Jonsson, G. Mills, K. W. Jacobsen, "Nudged elastic band method for finding minimum energy paths of transitions", in *Classical and Quantum Dynamics in Condensed Phase Simulations*, World Scientific, Singapore, 1998, p. 385-404.

[41] E. Bitzek, P. Koskinen, F. Gähler, M. Moseler, "Structural relaxation made simple", *Phys. Rev. Lett.* **97** (2006), article no. 170201.

[42] J. Guénolé, W. G. Nöhring, A. Vaid, F. Houllé, Z. Xie, A. Prakash, E. Bitzek, "Assessment and optimization of the fast inertial relaxation engine (FIRE) for energy minimization in atomistic simulations and its implementation in lammps", *Comput. Mater. Sci.* **175** (2020), article no. 109584.

[43] N. Mousseau, G. T. Barkema, "Traveling through potential energy landscapes of disordered materials: the activation-relaxation technique", *Phys. Rev. E* **57** (1998), no. 2, p. 2419-2424.

[44] T. Zhu, J. Li, A. Samanta, A. Leach, K. Gall, "Temperature and strain-rate dependence of surface dislocation nucleation", *Phys. Rev. Lett.* **100** (2008), no. 2, article no. 025502.

[45] C. R. Weinberger, A. T. Jennings, K. Kang, J. R. Greer, "Atomistic simulations and continuum modeling of dislocation nucleation and strength in gold nanowires", *J. Mech. Phys. Solids* **60** (2012), no. 1, p. 84-103.

[46] Q.-J. Li, B. Xu, S. Hara, J. Li, E. Ma, "Sample-size-dependent surface dislocation nucleation in nanoscale crystals", *Acta Mater.* **145** (2018), p. 19-29.

[47] J. Amodeo, E. Maras, D. Rodney, "Site dependence of surface dislocation nucleation in ceramic nanoparticles" (in press), to be published in *npj Computational Materials*, 2021.

[48] O. Kovalenko, C. Brandl, L. Klinger, E. Rabkin, "Self-healing and shape memory effects in gold microparticles through the defects-mediated diffusion", *Adv. Sci.* **4** (2017), no. 8, article no. 1700159.

[49] S. Plimpton, "Fast parallel algorithms for short-range molecular-dynamics", *J. Comput. Phys.* **117** (1995), no. 1, p. 1-19.

[50] S. A. S. Asif, K. J. Wahl, R. J. Colton, "Nanoindentation and contact stiffness measurement using force modulation with a capacitive load-displacement transducer", *Rev. Sci. Instrum.* **70** (1999), no. 5, p. 2408-2413.

[51] O. L. Warren, S. A. Downs, T. J. Wyrobek, "Challenges and interesting observations associated with feedback-controlled nanoindentation", *Zeitschrift für Metallkunde* **95** (2004), no. 5, p. 287-296.

[52] J.-J. Bian, G.-F. Wang, "Atomistic deformation mechanisms in copper nanoparticles", *J. Comput. Theor. Nanosci.* **10** (2013), no. 9, p. 2299-2303.

[53] J. Bian, X. Niu, H. Zhang, G. Wang, "Atomistic deformation mechanisms in twinned copper nanospheres", *Nanoscale Res. Lett.* **9** (2014), no. 1, p. 335-337.

[54] J. Amodeo, K. Lizoul, "Mechanical properties and dislocation nucleation in nanocrystals with blunt edges", *Mater. Des.* **135** (2017), p. 223-231.

[55] A. M. Goryaeva, C. Fusco, M. Bugnet, J. Amodeo, "Influence of an amorphous surface layer on the mechanical properties of metallic nanoparticles under compression", *Phys. Rev. Mater.* **3** (2019), no. 3, article no. 033606.

[56] D. Kilymis, C. Gerard, J. Amodeo, U. V. Waghmare, L. Pizzagalli, "Uniaxial compression of silicon nanoparticles: an atomistic study on the shape and size effects", *Acta Mater.* **158** (2018), p. 155-166.

[57] T. X. T. Sayle, B. J. Inkson, A. Karakoti, A. Kumar, M. Molinari, G. Möbus, S. C. Parker, S. Seal, D. C. Sayle, "Mechanical properties of ceria nanorods and nanochains; the effect of dislocations, grain-boundaries and oriented attachment", *Nanoscale* **3** (2011), no. 4, p. 1823-1837.

[58] F. Caddeo, A. Corrias, D. C. Sayle, "Tuning the properties of nanoceria by applying force: stress-induced ostwald ripening", *J. Phys. Chem. C* **120** (2016), no. 26, p. 14337-14344.

[59] T. F. Kelly, M. K. Miller, "Invited review article: Atom probe tomography", *Rev. Sci. Instrum.* **78** (2007), no. 3, article no. 031101.

[60] A. Prakash, J. Guenole, J. Wang, J. Müller, E. Spiecker, M. J. Mills, I. Povstugar, P. Choi, D. Raabe, E. Bitzek, "Atom probe informed simulations of dislocation-precipitate interactions reveal the importance of local interface curvature", *Acta Mater.* **92** (2015), p. 33-45.

[61] T. Persenot, G. Martin, R. Dendievel, J.-Y. Buffière, E. Maire, "Enhancing the tensile properties of EBM as-built thin parts: effect of HIP and chemical etching", *Mater. Charact.* **143** (2018), p. 82-93.

[62] M. Dupraz, G. Beutier, T. W. Cornelius, G. Parry, Z. Ren, S. Labat, M. I. Richard, G. A. Chahine, O. Kovalenko, M. De Boissieu, E. Rabkin, M. Verdier, O. Thomas, "3D imaging of a dislocation loop at the onset of plasticity in an indented nanocrystal", *Nano Lett.* **17** (2017), no. 11, p. 6696-6701.

[63] S. Roy, R. Gatti, B. Devincre, D. Mordehai, "A multiscale study of the size-effect in nanoindentation of Au nanoparticles", *Comput. Mater. Sci.* **162** (2019), p. 47-59.

[64] B. Devincre, L. P. Kubin, "Mesoscopic simulations of dislocations and plasticity", *Mater. Sci. Eng. A* **234** (1997), p. 8-14.

[65] M. Tang, M. Fivel, L. P. Kubin, "From forest hardening to strain hardening in body centered cubic single crystals: simulation and modeling", *Mater. Sci. Eng. A* **309–310** (2001), p. 256-260.

[66] V. Bulatov, L. Hsiung, M. Tang, A. Arsenlis, M. Bartelt, W. Cai, J. Florando, M. Hiratani, M. Rhee, G. Hommes, "Dislocation multi-junctions and strain hardening", *Nature* **440** (2006), no. 7088, p. 1174-1178.

[67] L. P. Kubin, *Dislocations, Mesoscale Simulations and Plastic Flow*, Oxford University Press, Oxford, 2013.

[68] E. Van der Giessen, A. Needleman, "Discrete dislocation plasticity: a simple planar model", *Model. Simul. Mater. Sci. Eng.* **3** (1995), no. 5, p. 689-735.

[69] M. Fivel, M. Verdier, G. Canova, "3D simulation of a nanoindentation test at a mesoscopic scale", *Mater. Sci. Eng. A* **234** (1997), p. 923-926.

[70] C. Lemarchand, J. L. Chaboche, B. Devincre, L. P. Kubin, "Multiscale modelling of plastic deformation", *J. Phys. IV* **09** (1999), no. PR9, p. Pr9-271-Pr9-277.

[71] A. Vattré, B. Devincre, F. Feyel, R. Gatti, S. Groh, O. Jamond, A. Roos, "Modelling crystal plasticity by 3D dislocation dynamics and the finite element method: the discrete-continuous model revisited", *J. Mech. Phys. Solids* **63** (2014), p. 491-505.

[72] Y. Cui, Z. Liu, Z. Zhuang, "Quantitative investigations on dislocation based discrete-continuous model of crystal plasticity at submicron scale", *Int. J. Plast.* **69** (2015), p. 54-72.

[73] O. Jamond, R. Gatti, A. Roos, B. Devincre, "Consistent formulation for the discrete-continuous model: improving complex dislocation dynamics simulations", *Int. J. Plast.* **80** (2016), p. 19-37.

[74] T. Mura, *Micromechanics of Defects in Solids*, Springer Science & Business Media, 1987.

[75] H.-J. Chang, M. Fivel, D. Rodney, M. Verdier, "Multiscale modelling of indentation in FCC metals: from atomic to continuum", *C. R. Phys.* **11** (2010), no. 3-4, p. 285-292.

[76] H. H. M. Cleveringa, E. Van der Giessen, A. Needleman, "Comparison of discrete dislocation and continuum plasticity predictions for a composite material", *Acta Mater.* **45** (1997), no. 8, p. 3163-3179.

[77] A. Vattré, B. Devincre, "Orientation dependence of plastic deformation in nickel-based single crystal superalloys: discrete-continuous model simulations", *Acta Mater.* **58** (2010), p. 1938-1951.

[78] V. S. Deshpande, A. Needleman, E. Van der Giessen, "Discrete dislocation modeling of fatigue crack propagation", *Acta Mater.* **50** (2002), no. 4, p. 831-846.

[79] M. D. Sangid, H. J. Maier, H. Sehitoglu, "The role of grain boundaries on fatigue crack initiation – An energy approach", *Int. J. Plast.* **27** (2011), no. 5, p. 801-821.

[80] S. Groh, B. Devincre, L. P. Kubin, A. Roos, F. Feyel, J. L. Chaboche, "Dislocations and elastic anisotropy in heteroepitaxial metallic thin films", *Phil. Mag. Lett.* **83** (2003), no. 5, p. 303-313.

[81] C. R. Weinberger, S. Aubry, S.-W. Lee, W. D. Nix, W. Cai, "Modelling dislocations in a free-standing thin film", *Model. Simul. Mater. Sci. Eng.* **17** (2009), no. 7, article no. 075007-27.

[82] J. A. El-Awady, S. I. Rao, C. Woodward, D. M. Dimiduk, M. D. Uchic, "Trapping and escape of dislocations in microcrystals with external and internal barriers", *Int. J. Plast.* **27** (2011), no. 3, p. 372-387.

[83] Y. Cui, G. Po, N. Ghoniem, "Size-tuned plastic flow localization in irradiated materials at the submicron scale", *Phys. Rev. Lett.* **120** (2018), no. 21, article no. 215501.

[84] S. Bel Haj Salah, "Plasticité des nanoparticules métalliques Cubiques à Faces Centrées", PhD Thesis, Ecole Nationale Supérieure de Mécanique et d'Aérotechnique, France, 2018.

[85] P. Armstrong, W. Peukert, "Size effects in the elastic deformation behavior of metallic nanoparticles", *J. Nanopart. Res.* **14** (2012), no. 12, article no. 1288.

[86] A. Hazarika, E. Peretz, V. Dikovsky, P. Santra, R. Shneck, D. Sarma, Y. Manassen, "STM verification of the reduction of the Young's modulus of CdS nanoparticles at smaller sizes", *Surf. Sci.* **630** (2014), p. 89-95.

[87] K. L. Johnson, *Contact Mechanics*, Cambridge University Press, Cambridge, 1987.

[88] B. Luan, M. O. Robbins, "The breakdown of continuum models for mechanical contacts", *Nature* **435** (2005), no. 7044, p. 929-932.

[89] G. Wang, J. Bian, J. Feng, X. Feng, "Compressive behavior of crystalline nanoparticles with atomic-scale surface steps", *Mater. Res. Express* **2** (2015), no. 1, article no. 015006.

[90] D. Kilymis, C. Gerard, L. Pizzagalli, "Ductile deformation of core-shell Si-SiC nanoparticles controlled by shell thickness", *Acta Mater.* **164** (2019), p. 560-567.

[91] Y. Hong, N. Zhang, M. A. Zaeem, "Metastable phase transformation and deformation twinning induced hardening-stiffening mechanism in compression of silicon nanoparticles", *Acta Mater.* **145** (2018), p. 8-18.

[92] L. M. Hale, X. Zhou, J. A. Zimmerman, N. R. Moody, R. Ballarini, W. W. Gerberich, "Phase transformations, dislocations and hardening behavior in uniaxially compressed silicon nanospheres", *Comput. Mater. Sci.* **50** (2011), no. 5, p. 1651-1660.

[93] D. Chrobak, N. Tymiak, A. Beaber, O. Ugurlu, W. Gerberich, R. Nowak, "Deconfinement leads to changes in the nanoscale plasticity of silicon", *Nat. Nanotechnol.* **6** (2011), p. 480-484.

[94] P. Valentini, W. W. Gerberich, T. Dumitrica, "Phase-transition plasticity response in uniaxially compressed silicon nanospheres", *Phys. Rev. Lett.* **99** (2007), no. 17, article no. 175701-4.

[95] Y. Feruz, D. Mordehai, "Towards a universal size-dependent strength of face-centered cubic nanoparticles", *Acta Mater.* **103** (2016), p. 433-441.

[96] J. Bian, H. Zhang, X. Niu, G. Wang, "Anisotropic deformation in the compressions of single crystalline copper nanoparticles", *Crystals* **8** (2018), no. 3, article no. 116.

[97] L. Yang, J.-J. Bian, G.-F. Wang, "Impact of atomic-scale surface morphology on the size-dependent yield stress of gold nanoparticles", *J. Phys. D: Appl. Phys.* **50** (2017), no. 24, article no. 245302-6.

[98] K. Shreiber, D. Mordehai, "Dislocation-nucleation-controlled deformation of Ni₃Al nanocubes in molecular dynamics simulations", *Model. Simul. Mater. Sci. Eng.* **23** (2015), article no. 085004.

[99] J. Amodeo, E. Bitzek, C. Begau, "Atomistic simulations of compression tests on Ni₃Al nanocubes", *Mater. Res. Lett.* **2** (2014), no. 3, p. 140-145.

[100] D. Chachamovitz, D. Mordehai, "The stress-dependent activation parameters for dislocation nucleation in molybdenum nanoparticles", *Sci. Rep.* **8** (2018), no. 1, article no. 3915.

[101] A. Sharma, R. Kositski, O. Kovalenko, D. Mordehai, E. Rabkin, "Giant shape- and size-dependent compressive strength of molybdenum nano- and microparticles", *Acta Mater.* **198** (2020), p. 72-84.

[102] J. J. Bian, L. Yang, X. R. Niu, G. F. Wang, "Orientation-dependent deformation mechanisms of bcc niobium nanoparticles", *Philos. Mag. A* **98** (2018), p. 1-17.

[103] Q. Yu, L. Qi, R. K. Mishra, X. Zeng, A. M. Minor, "Size-dependent mechanical properties of Mg nanoparticles used for hydrogen storage", *Appl. Phys. Lett.* **106** (2015), no. 26, article no. 261903-6.

[104] W. W. Gerberich, W. M. Mook, M. J. Cordill, C. B. Carter, C. R. Perrey, J. V. Heberlein, S. L. Girshick, "Reverse plasticity in single crystal silicon nanospheres", *Int. J. Plast.* **21** (2005), no. 12, p. 2391-2405.

[105] S. Bel Haj Salah, C. Gerard, L. Pizzagalli, "Influence of surface atomic structure on the mechanical response of aluminum nanospheres under compression", *Comput. Mater. Sci.* **129** (2017), p. 273-278.

[106] S. Brochard, P. Hirel, L. Pizzagalli, J. Godet, "Elastic limit for surface step dislocation nucleation in face-centered cubic metals: temperature and step height dependence", *Acta Mater.* **58** (2010), no. 12, p. 4182-4190.

[107] J. Schloesser, J. Roesler, D. Mukherji, "Deformation behaviour of freestanding single-crystalline Ni₃Al-based nanoparticles", *Int. J. Mater. Res.* **102** (2011), no. 5, p. 532-537.

[108] A. Sharma, N. Gazit, L. Klinger, E. Rabkin, "Pseudoelasticity of metal nanoparticles is caused by their ultrahigh strength", *Adv. Funct. Mater.* **30** (2019), no. 18, article no. 1807554.

[109] J. D. Nowak, A. R. Beaber, O. Ugurlu, S. L. Girshick, W. W. Gerberich, "Small size strength dependence on dislocation nucleation", *Scr. Mater.* **62** (2010), no. 11, p. 819-822.

[110] D. Mordehai, O. David, R. Kositski, "Nucleation-controlled plasticity of metallic nanowires and nanoparticles", *Adv. Mater.* **305** (2018), article no. 1706710-17.

[111] J. Glucklich, L. J. Cohen, "Size as a factor in the brittle-ductile transition and the strength of some materials", *Int. J. Fract. Mech.* **3** (1967), no. 4, p. 278-289.

[112] B. L. Karihaloo, "A note on complexities of compression failure", *Proc. R. Soc. A* **368** (1979), no. 1735, p. 483-493.

[113] J. T. Hagan, "Impossibility of fragmenting small particles: brittle–ductile transition", *J. Mater. Sci.* **16** (1981), no. 10, p. 2909-2911.

[114] Y. Yang, C.-C. Chen, M. C. Scott, C. Ophus, R. Xu, A. Pryor, L. Wu, F. Sun, W. Theis, J. Zhou, M. Eisenbach, P. R. C. Kent, R. F. Sabirianov, H. Zeng, P. Ercius, J. Miao, "Deciphering chemical order/disorder and material properties at the single-atom level", *Nature* **542** (2017), no. 7639, p. 75-79.

[115] H. Van Swygenhoven, P. M. Derlet, A. G. Frøseth, "Stacking fault energies and slip in nanocrystalline metals", *Nat. Mater.* **3** (2004), no. 6, p. 399-403.

[116] R. Kositski, O. Kovalenko, S.-W. Lee, J. R. Greer, E. Rabkin, D. Mordehai, "Cross-split of dislocations: an athermal and rapid plasticity mechanism", *Sci. Rep.* **6** (2016), no. 1, article no. 25966-8.

[117] D. Mordehai, Personnal Communication.

[118] J. Wang, Z. Zeng, C. R. Weinberger, Z. Zhang, T. Zhu, S. X. Mao, "In situ atomic-scale observation of twinning-dominated deformation in nanoscale body-centred cubic tungsten", *Nat. Mater.* **14** (2015), no. 6, p. 594-600.

[119] L. Proville, D. Rodney, M.-C. Marinica, "Quantum effect on thermally activated glide of dislocations", *Nat. Mater.* **11** (2012), no. 10, p. 845-849.

[120] K. Srivastava, R. Gröger, D. Weygand, P. Gumbsch, "Dislocation motion in tungsten: atomistic input to discrete dislocation simulations", *Int. J. Plast.* **47** (2013), p. 126-142.

[121] C. Marichal, K. Srivastava, D. Weygand, S. Van Petegem, D. Grolimund, P. Gumbsch, H. Van Swygenhoven, "Origin of anomalous slip in tungsten", *Phys. Rev. Lett.* **113** (2014), no. 2, article no. 025501.

[122] L. Dezerald, D. Rodney, E. Clouet, L. Ventelon, F. Willaime, "Plastic anisotropy and dislocation trajectory in BCC metals", *Nat. Commun.* **7** (2016), no. 1, article no. 11695.

[123] A. Kraych, E. Clouet, L. Dezerald, L. Ventelon, F. Willaime, D. Rodney, "Non-glide effects and dislocation core fields in BCC metals", *NPJ Comput. Mater.* **5** (2019), no. 1, p. 1237-1238.

[124] J. Amodeo, F. Pietrucci, J. Lam, "Out-of-equilibrium polymorph selection in nanoparticle freezing", *J. Phys. Chem. Lett.* **11** (2020), no. 19, p. 8060-8066.

[125] D. Pope, S. Ezz, "Mechanical properties of Ni_3AI and nickel-base alloys with high volume fraction of γ'", *Int. Met. Rev.* **29** (1984), no. 1, p. 136-167.

[126] R. C. Reed, *The Superalloys: Fundamentals and Applications*, Cambridge University Press, New York, 2008.

[127] L. Kovarik, R. R. Unocic, J. Li, P. Sarosi, C. Shen, Y. Wang, M. J. Mills, "Microtwinning and other shearing mechanisms at intermediate temperatures in Ni-based superalloys", *Prog. Mater. Sci.* **54** (2009), no. 6, p. 839-873.

[128] R. R. Unocic, N. Zhou, L. Kovarik, C. Shen, Y. Wang, M. J. Mills, "Dislocation decorrelation and relationship to deformation microtwins during creep of a γ' precipitate strengthened Ni-based superalloy", *Acta Mater.* **59** (2011), no. 19, p. 7325-7339.

[129] L. Pizzagalli, J. Godet, J. Guénolé, S. Brochard, "Dislocation cores in silicon: new aspects from numerical simulations", *J. Phys. Conf. Ser.* **281** (2011), no. 1, article no. 012002.

[130] D. Rodney, L. Ventelon, E. Clouet, L. Pizzagalli, F. Willaime, "Ab initio modeling of dislocation core properties in metals and semiconductors", *Acta Mater.* **124** (2017), p. 633-659.

[131] N. Zhang, Q. Deng, Y. Hong, L. Xiong, S. Li, M. Strasberg, W. Yin, Y. Zou, C. R. Taylor, G. Sawyer, Y. Chen, "Deformation mechanisms in silicon nanoparticles", *J. Appl. Phys.* **109** (2011), no. 6, article no. 063534.

[132] L. M. Hale, D. B. Zhang, X. Zhou, J. A. Zimmerman, N. R. Moody, T. Dumitrica, R. Ballarini, W. W. Gerberich, "Dislocation morphology and nucleation within compressed Si nanospheres: a molecular dynamics study", *Comput. Mater. Sci.* **54** (2012), p. 280-286.

[133] K.-C. Fang, C.-I. Weng, S.-P. Ju, "An investigation into the mechanical properties of silicon nanoparticles using molecular dynamics simulations with parallel computing", *J. Nanopart. Res.* **11** (2009), no. 3, p. 581-588.

[134] E. Maras, L. Pizzagalli, T. Ala-Nissila, H. Jonsson, "Atomic scale formation mechanism of edge dislocation relieving lattice strain in a GeSi overlayer on Si(001)", *Sci. Rep.* **7** (2017), no. 1, article no. 11966.

[135] J. Guenole, S. Brochard, J. Godet, "Unexpected slip mechanism induced by the reduced dimensions in silicon nanostructures: atomistic study", *Acta Mater.* **59** (2011), no. 20, p. 7464-7472.

[136] J. Amodeo, S. Merkel, C. Tromas, P. Carrez, S. Korte-Kerzel, P. Cordier, J. Chevalier, "Dislocations and plastic deformation in MgO crystals: a review", *Crystals* **8** (2018), no. 6, p. 240-253.

[137] C. Hulse, J. Pask, "Mechanical properties of magnesia single crystals compression", *J. Am. Ceram. Soc.* **43** (1960), no. 7, p. 373-378.

[138] C. Hulse, S. Copley, J. Pask, "Effect of crystal orientation on plastic deformation of magnesium oxide", *J. Am. Ceram. Soc.* **46** (1963), no. 7, p. 317-323.

[139] S. Korte, W. Clegg, "Discussion of the dependence of the effect of size on the yield stress in hard materials studied by microcompression of MgO", *Philos. Mag. A* **91** (2011), no. 7-9, p. 1150-1162.

[140] J. Amodeo, P. Carrez, B. Devincre, P. Cordier, "Multiscale modelling of MgO plasticity", *Acta Mater.* **59** (2011), no. 6, p. 2291-2301.

[141] D. C. Sayle, S. A. Maicaneanu, G. W. Watson, "Atomistic models for CeO_2 (111), (110), and (100) nanoparticles, supported on yttrium-stabilized zirconia", *J. Am. Chem. Soc.* **124** (2002), no. 38, p. 11429-11439.

[142] G. Möbus, Z. Saghi, D. C. Sayle, U. M. Bhatta, A. Stringfellow, T. X. T. Sayle, "Dynamics of polar surfaces on ceria nanoparticles observed in situ with single-atom resolution", *Adv. Funct. Mater.* **21** (2011), no. 11, p. 1971-1976.

[143] T. X. T. Sayle, M. Molinari, S. Das, U. M. Bhatta, G. Möbus, S. C. Parker, S. Seal, D. C. Sayle, "Environment-mediated structure, surface redox activity and reactivity of ceria nanoparticles", *Nanoscale* **5** (2013), no. 13, article no. 6063-11.

[144] K. Reed, A. Cormack, A. Kulkarni, M. Mayton, D. Sayle, F. Klaessig, B. Stadler, "Exploring the properties and applications of nanoceria: is there still plenty of room at the bottom?", *Environ. Sci.: Nano* **1** (2014), no. 5, p. 390-405.

[145] P. Sarobol, M. Chandross, J. D. Carroll, W. M. Mook, D. C. Bufford, B. L. Boyce, K. Hattar, P. G. Kotula, A. C. Hall,

"Room temperature deformation mechanisms of alumina particles observed from in situ micro-compression and atomistic simulations", *J. Therm. Spray Technol.* **25** (2015), no. 1, p. 82-93.

[146] A. H. De Aza, J. Chevalier, G. Fantozzi, M. Schehl, R. Torrecillas, "Crack growth resistance of alumina, zirconia and zirconia toughened alumina ceramics for joint prostheses", *Biomaterials* **23** (2002), no. 3, p. 937-945.

[147] D. Mordehai, E. Rabkin, D. J. Srolovitz, "Pseudoelastic deformation during nanoscale adhesive contact formation", *Phys. Rev. Lett.* **107** (2011), no. 9, p. 449-454.

[148] A. T. Jennings, J. Li, J. R. Greer, "Emergence of strain-rate sensitivity in Cu nanopillars: transition from dislocation multiplication to dislocation nucleation", *Acta Mater.* **59** (2011), no. 14, p. 5627-5637.

[149] R. Tenne, L. Rapoport, Y. Bilik, Y. Feldman, M. Homyonfer, S. R. Cohen, "Hollow nanoparticles of WS_2 as potential solid-state lubricants", *Nature* **387** (1997), no. 6635, p. 791-793.

[150] H. J. Fan, U. Gösele, M. Zacharias, "Formation of nanotubes and hollow nanoparticles based on kirkendall and diffusion processes: a review", *Small* **3** (2007), no. 10, p. 1660-1671.

[151] J. J. Teo, Y. Chang, H. C. Zeng, "Fabrications of hollow nanocubes of Cu_2O and Cu via reductive self-assembly of CuO nanocrystals", *Langmuir* **22** (2006), no. 17, p. 7369-7377.

[152] N. Gazit, L. Klinger, G. Richter, E. Rabkin, "Formation of hollow gold-silver nanoparticles through the surface diffusion induced bulk intermixing", *Acta Mater.* **117** (2016), p. 188-196.

[153] S. Ozden, C. S. Tiwary, J. Yao, G. Brunetto, S. Bhowmick, S. Asif, R. Vajtai, P. M. Ajayan, "Highly ordered carbon-based nanospheres with high stiffness", *Carbon* **105** (2016), p. 144-150.

[154] Z. W. Shan, G. Adesso, A. Cabot, M. P. Sherburne, S. A. S. Asif, O. L. Warren, D. C. Chrzan, A. M. Minor, A. P. Alivisatos, "Ultrahigh stress and strain in hierarchically structured hollow nanoparticles", *Nat. Mater.* **7** (2008), no. 12, p. 947-952.

[155] R. P. Chaukulkar, K. de Peuter, P. Stradins, S. Pylypenko, J. P. Bell, Y. Yang, S. Agarwal, "Single-step plasma synthesis of carbon-coated silicon nanoparticles", *ACS Appl. Mater. Inter.* **6** (2014), no. 21, p. 19026-19034.

[156] K. L. Firestein, D. G. Kvashnin, A. M. Kovalskii, Z. I. Popov, P. B. Sorokin, D. V. Golberg, D. V. Shtansky, "Compressive properties of hollow BN nanoparticles: theoretical modeling and testing using a high-resolution transmission electron microscope", *Nanoscale* **10** (2018), no. 17, p. 8099-8105.

[157] W. Yang, S. Mao, J. Yang, T. Shang, H. Song, J. Mabon, W. Swiech, J. R. Vance, Z. Yue, S. J. Dillon, H. Xu, B. Xu, "Large-deformation and high-strength amorphous porous carbon nanospheres", *Sci. Rep.* **6** (2016), no. 1, article no. 24187.

[158] W. Gonçalves, J. Amodeo, J. Morthomas, P. Chantrenne, M. Perez, G. Foray, C. L. Martin, "Nanocompression of secondary particles of silica aerogel", *Scr. Mater.* **157** (2018), p. 157-161.

[159] D. Kilymis, C. Gerard, L. Pizzagalli, "Mechanical properties of amorphous silicon nanoparticles", in *TMS 2019 148th Annual Meeting & Exhibition Supplemental Proceedings*, The Minerals, Metals & Materials Series, Springer, Berlin, Heidelberg, 2019, p. 1347-1354.

[160] H. K. Issa, A. Taherizadeh, A. Maleki, "Atomistic-level study of the mechanical behavior of amorphous and crystalline silica nanoparticles", *Ceram. Int.* **46** (2020), no. 13, p. 21647-21656.

[161] J. Zhao, S. Nagao, G. M. Odegard, Z. Zhang, H. Kristiansen, J. He, "Size-dependent mechanical behavior of nanoscale polymer particles through coarse-grained molecular dynamics simulation", *Nanoscale Res. Lett.* **8** (2013), no. 1, article no. 541.

[162] E. W. Bucholz, S. B. Sinnott, "Computational investigation of the mechanical and tribological responses of amorphous carbon nanoparticles", *J. Appl. Phys.* **113** (2013), no. 7, article no. 073509.

[163] L. Pascazio, J. W. Martin, K. Bowal, J. Akroyd, M. Kraft, "Exploring the internal structure of soot particles using nanoindentation: a reactive molecular dynamics study", *Combus. Flame* **219** (2020), p. 45-56.

[164] I. Z. Jenei, F. Dassenoy, T. Epicier, A. Khajeh, A. Martini, D. Uy, H. Ghaednia, A. Gangopadhyay, "Mechanical characterization of diesel soot nanoparticles: in situ compression in a transmission electron microscope and simulations", *Nanotechnology* **29** (2018), no. 8, article no. 085703.

[165] M. J. Demkowicz, A. S. Argon, "Liquidlike atomic environments act as plasticity carriers in amorphous silicon", *Phys. Rev. B* **72** (2005), no. 24, article no. 245205.

[166] C. Fusco, T. Albaret, A. Tanguy, "The role of local order in the small-scale plasticity of model amorphous materials", *Phys. Rev. E* **82** (2010), article no. 066116.

[167] L. Yang, J. J. Bian, H. Zhang, X. R. Niu, G. F. Wang, "Size-dependent deformation mechanisms in hollow silicon nanoparticles", *AIP Adv.* **5** (2015), no. 7, article no. 077162.

[168] J. Wu, S. Nagao, Z. Zhang, J. He, "Deformation and fracture of nano-sized metal-coated polymer particles: a molecular dynamics study", *Eng. Fract. Mech.* **150** (2015), p. 209-221.

[169] R. A. Fleming, M. Zou, "The effects of confined core volume on the mechanical behavior of Al/a-Si core-shell nanostructures", *Acta Mater.* **128** (2017), p. 149-159.

[170] F. J. Valencia, B. Pinto, M. Kiwi, C. J. Ruestes, E. M. Bringa, J. Rogan, "Nanoindentation of polycrystalline Pd hollow nanoparticles: grain size role", *Comput. Mater. Sci.* **179** (2020), article no. 109642.

[171] F. Xu, T. Kobayashi, Z. Yang, T. Sekine, H. Chang, N. Wang, Y. Xia, Y. Zhu, "How the toughest inorganic fullerene

cages absorb shockwave pressures in a protective nanocomposite: experimental evidence from two in situ investigations", *ACS Nano* **11** (2017), no. 8, p. 8114-8121.

[172] J. Pokluda, M. Černý, P. Šandera, M. Šob, "Calculations of theoretical strength: state of the art and history", *J. Comput.-Aided Mater. Des.* **11** (2004), no. 1, p. 1-28.

[173] N. Bertin, R. B. Sills, W. Cai, "Frontiers in the simulation of dislocations", *Annu. Rev. Mater. Res.* **50** (2020), no. 1, p. 437-464.

[174] A. F. Voter, F. Montalenti, T. C. Germann, "Extending the time scale in atomistic simulation of materials", *Annu. Rev. Mater. Res.* **32** (2002), p. 321-346.

[175] D. Perez, B. P. Uberuaga, Y. Shim, J. G. Amar, A. F. Voter, "Chapter 4 accelerated molecular dynamics methods: introduction and recent developments" (R. A. Wheeler, ed.), Annual Reports in Computational Chemistry, no. Supplement C, vol. 5, Elsevier, 2009, p. 79-98.

[176] W. Gerberich, E. B. Tadmor, J. Kysar, J. A. Zimmerman, A. M. Minor, I. Szlufarska, J. Amodeo, B. Devincre, E. Hintsala, R. Ballarini, "Review article: case studies in future trends of computational and experimental nanomechanics", *J. Vac. Sci. Technol. A* **35** (2017), no. 6, article no. 060801-0.

[177] L. A. Zepeda-Ruiz, A. Stukowski, T. Oppelstrup, V. V. Bulatov, "Probing the limits of metal plasticity with molecular dynamics simulations", *Nat. Mater.* **550** (2017), p. 1-18.

[178] J. Behler, "Perspective: machine learning potentials for atomistic simulations", *J. Chem. Phys.* **145** (2016), no. 17, article no. 170901.

[179] F. Fan, S. Huang, H. Yang, M. Raju, D. Datta, V. B. Shenoy, A. C. T. van Duin, S. Zhang, T. Zhu, "Mechanical properties of amorphous Li x Si alloys: a reactive force field study", *Model. Simul. Mater. Sci. Eng.* **21** (2013), no. 7, article no. 074002.

[180] T. Liang, T.-R. Shan, Y.-T. Cheng, B. D. Devine, M. Noordhoek, Y. Li, Z. Lu, S. R. Phillpot, S. B. Sinnott, "Classical atomistic simulations of surfaces and heterogeneous interfaces with the charge-optimized many body (COMB) potentials", *Mater. Sci. Eng. R. Rep.* **74** (2013), no. 9, p. 255-279.

[181] P. Koskinen, V. Mäkinen, "Density-functional tight-binding for beginners", *Comput. Mater. Sci.* **47** (2009), no. 1, p. 237-253.

[182] M. T. Kiani, Y. Wang, N. Bertin, W. Cai, X. W. Gu, "Strengthening mechanism of a single precipitate in a metallic nanocube", *Nano Lett.* **19** (2019), no. 1, p. 255-260.